REPORT DOCUMENTATION PAGE

1a REPOR
UNCL

2a SECURI

2b DECLA

# AD-A205 110

1b RESTRICTIVE MARKINGS
NONE

3 DISTRIBUTION/AVAILABILITY OF REPORT
Approved for public release.
Distribution unlimited.

4 PERFORMING ORGANIZATION REPORT NUMBER(S)
Technical Report No. 12

5 MONITORING ORGANIZATION REPORT NUMBER(S)

6a NAME OF PERFORMING ORGANIZATION
Massachusetts Institute of Technology

6b OFFICE SYMBOL (If applicable)

7a NAME OF MONITORING ORGANIZATION
ONR

6c. ADDRESS (City, State, and ZIP Code)
77 Massachusetts Avenue, Room 1-306
Cambridge, MA 02139

7b. ADDRESS (City, State, and ZIP Code)
800 North Quincy Street
Arlington, VA 22217

8a. NAME OF FUNDING/SPONSORING ORGANIZATION
DARPA

8b. OFFICE SYMBOL (If applicable)

9. PROCUREMENT INSTRUMENT IDENTIFICATION NUMBER
N00014-86-K-0768

8c. ADDRESS (City, State, and ZIP Code)
1400 Wilson Boulevard
Arlington, VA 22209

10 SOURCE OF FUNDING NUMBERS

| PROGRAM ELEMENT NO. | PROJECT NO. | TASK NO. | WORK UNIT ACCESSION NO. |
|---|---|---|---|
| R & T Code | A 400005 | | |

11. TITLE (Include Security Classification)
TOPOLOGICAL FEATURES OF STRUCTURAL RELAXATIONS IN A TWO-DIMENSIONAL MODEL ATOMIC GLASS-II

12. PERSONAL AUTHOR(S) Deng, Derguo; Argon, Ali S.; and Yip, Sidney

| 13a. TYPE OF REPORT | 13b TIME COVERED | 14. DATE OF REPORT (Year, Month, Day) | 15. PAGE COUNT |
|---|---|---|---|
| Interim technical | FROM 1987 TO 1988 | 1989 January 23 | 60 |

16. SUPPLEMENTARY NOTATION
Submitted for publication in Phil. Transactions of the Royal Society

| 17 COSATI CODES | | |
|---|---|---|
| FIELD | GROUP | SUB-GROUP |
| | | |
| | | |

18. SUBJECT TERMS (Continue on reverse if necessary and identify by block number)
Structural relaxations, in amorphous media; computer simulation. (mgm)

19. ABSTRACT (Continue on reverse if necessary and identify by block number)

The topological features of atom motions in a high-temperature melt, a subcooled melt above $T_g$, and a glass below $T_g$, were analysed in detail by means of a two-dimensional molecular dynamics simulation. A striking analogy was observed between the structure and properties of the liquid-like material separating quasi-ordered domains of atom clusters, and high angle grain boundaries. The main feature of the structural relaxation below the melting point, both above and below $T_g$ was the gradual dissolution and disappearance of the liquid-like material, permitting increasing order in the previously quasi-ordered domains and a growth in their sizes. In these processes, many sequences reminiscent of cancellation of dislocation pairs, or mutual reactions to give more stable sets were observed.

20 DISTRIBUTION/AVAILABILITY OF ABSTRACT
☒ UNCLASSIFIED/UNLIMITED ☐ SAME AS RPT ☐ DTIC USERS

21. ABSTRACT SECURITY CLASSIFICATION
Unclassified

| 22a NAME OF RESPONSIBLE INDIVIDUAL | 22b TELEPHONE (Include Area Code) | 22c. OFFICE SYMBOL |
|---|---|---|
| Dr. JoAnn Millikan | (202) 696-4410 | |

DD FORM 1473, 84 MAR 83 APR edition may be used until exhausted.
All other editions are obsolete

SECURITY CLASSIFICATION OF THIS PAGE

# TOPOLOGICAL FEATURES OF STRUCTURAL RELAXATIONS IN A TWO-DIMENSIONAL MODEL ATOMIC GLASS - II

**D. Deng [1], A.S. Argon, and S. Yip**

**Massachusetts Institute of Technology, Cambridge, MA 02139**

**U.S.A.**

## Abstract

*The topological features of atom motions in a high-temperature melt, a sub-cooled melt above $T_g$, and a glass below $T_g$, were analysed in detail by means of a two-dimensional molecular dynamics simulation. A striking analogy was observed between the structure and properties of the liquid-like material separating quasi-ordered domains of atom clusters, and high angle grain boundaries. The main feature of the structural relaxation below the melting point, both above and below $T_g$ was the gradual dissolution and disappearance of the liquid-like material, permitting increasing order in the previously quasi-ordered domains and a growth in their sizes. In these processes, many sequences reminiscent of cancellation of dislocation pairs, or mutual reactions to give more stable sets were observed.*



[1] On leave from the Institute for Precious Metals in Kunming, Yunnan Province, China.

# I. INTRODUCTION

The resistance to inelastic deformation of amorphous metallic and polymeric materials depends on the state of aging of their structure, i.e., the degree of completion of structural relaxation. Such structural relaxations have been widely studied experimentally by many techniques, which include: direct probing using X-ray scattering [1], decay of excess enthalpy by calorimetry and related means [2], and indirect probing through the effect of aging on mechanical properties, such as internal friction [3-5], viscous flow [6], micro hardness [4,7], in both amorphous metals, and in polymers [8]. While such structural relaxations have been characterized quite well through changing structural parameters, such as radial distribution functions (RDF), etc., the actual kinematics of the local relaxation processes, which produce both topological and chemical short range order, are not well understood. Not much is known about how these processes are related to the experimentally observed kinetics of relaxation. Since inelastic deformation in amorphous media preferentially selects the portion of the volume of excess properties, such kinematical features of the relaxation are of primary interest. Because these processes are complex, inhomogeneous, and very local, computer simulations using the molecular dynamics (MD) or the Monte Carlo (MC) approaches should be promising for their visualization. In the past, Takeuchi and coworkers [9,10] have performed such simulations for $Cu_xZr_{1-x}$ type glasses in three-dimensional models and have reported that the principal driving force for the relaxations is the excess in atomic level

deviatoric stresses, and that the principal result is the development of chemical short range order. Kobayashi and Takeuchi [10] have also given additional information on the changing distributions of atomic level, mean normal stress, and some atomic displacement fields that accompany the structural relaxation process. In spite of these useful observations, both the kinematics of local rearrangements and associated kinetics remain inadequately understood in relating the changing structure to its deformation resistance through local mechanisms. We have now carried out a more complete MD simulation using the same truncated $Cu - Zr$ pair potentials used by Kobayashi et al. [11], but in a two-dimensional cell using periodic boundary conditions to better visualize the topological features of the structure. In a preceding communication [12], to be referred to here as (I), we reported results of a simulation of the melting and glass transition process in a two-dimensional ideal material held together by the same pair potential. In this, and a following communication [13], to be referred to here as (III), we report respectively the topological features and the details of the kinetics of structural relaxations.

## II. DETAILS OF THE SIMULATION

### *2.1 The molecular Dynamics Method*

The details of the molecular dynamics method that was used in the present simulation were described in more detail in (I). There, it was shown that single component materials are too unstable in the amorphous solid, and

crystallize exceedingly rapidly, but that two-component solids with appropriate size ratios such as $Cu$ and $Zr$, are considerably more stable and do not crystallize as rapidly when relaxed at low temperature, making them more suitable for studies of structural relaxations. Thus, the present simulation uses the same two-dimensional cell under periodic boundary conditions of a $Cu_{0.5}Zr_{0.5}$ type solid held together with a 4-8 type truncated Lennard-Jones potential, as was described in (I). There, it was shown that the fundamental time constant of the atomic period of this material was $\eta = (mr_o^2/E_o)^{0.5} = 5.40\text{x}10^{-13}$sec., and that under an external normalized pressure of $p^* = 1.0$[(•)] the material melts at a normalized temperature of $T_m^* = 0.25$ and undergoes a glass transition at a normalized temperature of 0.18. The time steps between different states in the integration of the equations of motion were 0.02 or $1.1\text{x}10^{-14}$sec. As in (I), in the present simulation, the magnitude of the so-called border mass used to stabilize the solutions and maintain the external pressure constant was 4. (See Appendix I of the accompanying communication (III) on the kinetics of structural relaxation [13] on the choice of border mass.)

---

(•)For nomenclature and definition of normalization terms, see the Appendix of (I).

## *2.2 Intensive State Parameters*

The amorphous medium and its state need to be described by a set of parameters. The ones that have been found most useful are: (a) the volume per atom $\Omega$, delineated in 2-D models readily by the Voronoi polygons constructed around each atom site, and the free volume, $s_f$, which is the excess of a local average in this volume over and above a certain reference volume for the entire field of polygons, (b) the atomic level stress tensor, $\sigma_{\alpha\beta}$, related directly to the distribution of material misfit in the amorphous material [14], (c) the atomic level elastic constants $C_{\alpha\beta\gamma\delta}$, related to the state of dilatation and shear of the local site, (d) the atomic level enthalpy, $h$, useful in describing the excess properties of an atomic site, and (e) the atomic site distortion parameter, $w$, giving a measure of the distortion of the local atomic site compared to an equiaxed site among uniform Voronoi polygons. We now define these parameters below.

### 2.2.1 The Voronoi polygons and free volume

In the 2-D material, which is the subject of this simulation, the volume per atom is represented by the area delineated by a polygon constructed around an atomic site by the perpendicular lines bisecting the lines connecting atom centers. In a perfect 2-D hexagonal material, all Voronoi polygons are hexagons. In (I), however, we showed that when an initially hexagonal 2-D material undergoes melting, many of the hexagonal polygons are transformed into pen-

tagons and heptagons, and that these two associate into structural dipoles of 5 and 7 sided polygon pairs, which in turn associate into strings that percolate through the simulation cell in the melt. While these alterations in the number of edges of the Voronoi polygons are the most dramatic manifestations of change, other corollary changes also occur in the number of edges meeting at corners of polygons, i.e., instead of only corners where 3 edges meet, other corners, where 4 edges meet also, appear with considerable regularity. The meaning of these special structural features and how they re-distribute themselves in the melt, or how they age out at lower temperatures, is the main subject of discussion in this communication.

Since significant increases in local dilatation results in substantial reductions in cohesive interaction, which has important consequences in the deformation of an amorphous solid, the excess in the local volume per atom over and above that in a reference material, is an important parameter of state. This local structure parameter, which is called the free volume, was evaluated in the two-dimensional model of the present simulation as

$$s_f(i) = \frac{1}{n}\sum_{i}^{n} s_i - s_o \quad , \tag{1}$$

where $s_i$ is the area of a Voronoi polygon, and the sum $n$ is carried out over the central atom and its nearest neighbors that enter into the definition of its Voronoi polygon faces. The reference area $s_o$ was taken as the average Voronoi

polygon area in the entire simulation cell.

### 2.2.2. The atomic level stress tensor

Egami and Vitek [14] have emphasized the utility of the atomic level stress tensor, defined much earlier by Born and Huang [15], to describe the large local variations of interatomic forces that result from the distributed material misfit that accompanies the amorphous state. The atomic level stress is defined as:

$$\sigma_{\alpha\beta}(i) = \frac{1}{2\Omega_i} \sum_{j \neq i} \left[ \frac{\partial \Phi(r)}{\partial r} \right]_{r=r_{ij}} \frac{r_{ij}^{\alpha} r_{ij}^{\beta}}{r_{ij}}, \tag{2}$$

where $\Phi$ is the truncated interatomic pair potential of the 4-8 Lennard-Jones type, introduced in (I), $r_{ij}$ is the magnitude of the radius vector connecting atoms $i$ and $j$, $r_{ij}^{\alpha}$ is the magnitude of the component in the local $\alpha$ direction of the vector connecting atoms $i$ and $j$, and $\Omega_i$ is the volume of the central atom occupying site $i$, for which the component of the stress tensor is being calculated. The sum is over all near neighbors $j$ surrounding the atom $i$, which are within the potential cutoff radius. In the present simulation here, as well as those in (III) and (IV), what will be of interest is not only the shear stress $\sigma_{xy}(i)$ referred to the principal axes of the undisturbed simulation cell, but also the maximum shear stress $\tau_i$ in the plane regardless of direction, and the atomic level pressure $p_i$, both defined as:

$$\tau_i = \sqrt{(\sigma_{xy}(i))^2 + \left(\frac{\sigma_{xx}(i) - \sigma_{yy}(i)}{2}\right)^2} \quad , \tag{3}$$

$$p_i = -\frac{1}{2}\left(\sigma_{xx}(i) + \sigma_{yy}(i)\right) \quad , \tag{4}$$

2.2.3 The atomic level elastic constants

In the amorphous medium, where large local variations in free volume exist, forcing the material into non-linear modes of response, there are important variations in the local elastic properties in the neighborhoods of each atomic site. These local moduli are characterized by an elastic constant tensor, which is defined as [16]:

$$C_{\alpha\beta\gamma\delta}(i) = \frac{\partial^2\Phi}{\partial\epsilon_{\alpha\beta}\partial\epsilon_{\gamma\delta}} = \frac{1}{2\Omega_i}\sum_{j\neq i}\left\{\left[\frac{1}{r}\frac{\partial\Phi}{\partial r}\right]_{r=r_{ij}}\delta_{\alpha\gamma} + \frac{r_{ij}^{\alpha}r_{ij}^{\gamma}}{(r_{ij})^2}\left[\frac{\partial^2\Phi}{\partial r^2} - \frac{1}{r}\frac{\partial\Phi}{\partial r}\right]_{r=r_{ij}}\right\} r_{ij}^{\beta}\ r_{ij}^{\delta} \quad , \tag{5}$$

where $\delta_{\alpha\gamma}$ is the Kronecker delta, and the sum on $j$ is again over all nearest neighbors, over which the truncation permits interactions. In Eqn. (5), $\epsilon_{\alpha\beta}$

and $\epsilon_{\gamma\delta}$ are tensor strain components, which are given only to define the elastic constants. They are not explicitly used here, and will therefore not be developed. In (IV), where imposed deformations are of interest, strains will be defined for use there [12].

### 2.2.4. Atomic level enthalpy

The excess enthalpy has long been identified to be an important characterizing parameter of amorphous materials, where it has been considered by many investigators as the principal driving force in structural relaxation. We define it as:

$$h(i) = \frac{1}{2}\sum_{j\neq i}\Phi(r_{ij}) + \frac{1}{2}mv_i^2 + p\Omega \quad . \tag{6}$$

### 2.2.5. The atomic site distortion parameters

Many Voronoi polygons in the melt and also in the unrelaxed glassy state are considerably distorted. These distortions are geometrical complements to the free volume. Although both evoke atomic level internal stresses and changes in elastic constants, their quantitative description provides additional visual evidence of the strong interactions in the "liquid-like" material between polygons which combine excess free volume and distortions. We define the site distortion

parameter $w(i)$ as the ratio of the perimeter length $\ell_i$ of the actual polygon to the circumference of a circle having the same area as the polygon, i.e.,

$$w(i) = \frac{\ell_i}{2\sqrt{\pi s_i}} \ , \tag{7}$$

where $s_i$ is the actual area of the polygon. Thus, for a circle $w(i) = 1.0$ by definition. This is the minimum value for any $w(i)$, and corresponds to the highest degree of symmetry that a polygon can have.

The site distortion parameter $w(i)$ increases with decreasing numbers of edges of a polygon for regular polygons. This is a trivial increase, which partially dilutes the more relevant and interesting increase that comes form true distortion. These trivial base level increases in $w_o$ for regular polygons are listed in Table I.

More importantly, the distortion parameter increases with increasing departure from regularity of a polygon. To separate the real site distortion from the background increases listed in Table I, it is useful to define a net site distortion parameter $w'(i)$, which gives the difference between the actual measured valued and the background value defined as:

$$w'(i) = w(i) - w_o \ , \tag{8}$$

for each polygon type.

The distortion parameter for each atom site complements the free volume information. The pair of factors of free volume $s_f(i)$ and site distortion parameter $w(i)$ are indirect structural parallels to the atomic level negative pressure and maximum shear stress.

### *2.3 The Structural Relaxation Simulation*

The initial state for the present simulation of structural fluctuations and relaxations was taken to be the state of the material in the melt at the melting point $T^* = 0.25$ for the 2-D, two-component $Cu - Zr$ alloy discussed in detail in (I). The process history for the present simulation of structural alterations is shown in Fig. 1, in which two complementary structural relaxations have been investigated: (a) a relaxation in the subcooled liquid region between $T_m$ and $T_g$, at a temperature of $T^* = 0.2$, and (b) a relaxation below $T_g$ at $T^* = 0.1$. In both of these cases, the material is suddenly cooled from the molten state at $T^* = 0.25$ (point E in Fig. 1) to the lower temperature. Thus, the cooling rate to the isothermal relaxation temperatures was infinite and was accomplished by suddenly decreasing the average kinetic energies of atoms in the simulation cell for the given initial coordinates in the melt.

We discuss, however, also in considerable detail, the nature of the disorder and its continued variation at $T^* = 0.3$ in the high-temperature melt to obtain

a better appreciation of the role of the liquid-like material in the behavior of the melt. All simulations were carried out at an external pressure of $p^* = 1.0$.

## III. RESULTS OF THE SIMULATION

### *3.1 Structural Defects in the Amorphous State*

In (I), we have demonstrated that in the amorphous state of the 2-D material above the melting point, in rapidly solidified form as a sub-cooled liquid, or in the glassy form below $T_g$, the disorder that is evident from the radial distribution functions (RDF) of atom positions is not uniformly spread over the entire material. Instead, there is a considerable fraction of the material which is in a reasonably well ordered form at any snapshot in time, being made up of more or less distorted hexagonal polygons. In the melt, these ordered regions were found separated by strings of "liquid-like" material percolating through the simulation cell. The liquid-like material in turn, making up a volume fraction of about 0.4, was found to be composed of primarily polygons of 5 and 7 sides, with occasional polygons with 4 and also 8 sides. In addition to this defective material separating more ordered domains, occasional dipoles of 5 and 7 sided polygons were also found inside the quasi-ordered domains. Such isolated dipoles of 5-7 sided polygons in the quasi-ordered domains were recognized as edge dislocations, which when somewhat displaced, could transform into two adjacent pentagons separated by a flat face from two adjacent large distorted hexagons, all sharing a four sided corner. This configuration was identified as

an edge dislocation in a metastable intermediate condition between two stable configurations made of 5-7 sided polygons. An associated study of the mutual arrangement of 5-7 sided polygon pairs established that most of such arrangements where two 5-7 sided polygon pairs face each other with the 7 sided polygons being near or next near neighbors and the 5 sided polygons being directed outward, are vacancies or vacancy clusters. On the other hand, the arrangement of the 5-7 sided polygon pairs in the liquid-like material strings separating quasi-ordered domains were found to have a high frequency of being ordered in sequences of touching....5-7-5-7....arrangements, with occasional interruptions breaking this sequence. Clearly, in a perfect hexagonal mat, such regions would constitute high angle grain boundaries, and in the amorphous material, they must be interpreted as the geometrically necessary arrangement of topological defects that result in the misorientation of the quasi-ordered regions which they separate. The common feature of all of these defects was recognized to be the local excess free volume which they provide, which was established to be on the average a fraction of 0.07 for the dipole of a 5-7 sided polygon pair.

In the amorphous material of the subcooled melt above $T_g$, the percolation condition of the liquid-like material was often found broken in snapshots in time, but re-established at times in between – most likely due to the decreasing misorientation between the quasi-ordered domains. Below the glass transition temperature, the percolation condition of the liquid-like material was always found broken.

### *3.2 Time Dependent Structural Variations in the Melt*

The processes of structural fluctuation occurring above the melting point at $T^* = 0.3$ were followed in some detail over a period of 500 time steps (25 thermal fluctuation periods). Figures 2a - 2c show three quite representative snapshots in time, after 300, 400, and 500 time steps. It is clear that the main topological feature is the more or less aligned strings of liquid-like material made by the association of 5-7 sided polygons, with a dominant alternating sequence of....5-7-5-7....arrangements. In addition to the presence of main chains of strings of polygon pairs, there were often side branches either joining on the main chain or at times forming isolated subsidiary chains. In addition, however, the somewhat more regular hexagonal regions which the strings separate were themselves quite markedly distorted. As discussed in (I), at this state of the material, the 2-D RDF shows only 3 broad and interconnected peaks, made up of the fusion of the second and third peaks, and the fourth and fifth peaks, in addition to the first peak. A certain number of 4 edged corners separating two neighboring 5 sided polygons were visible in all the frames. As discussed above, these are higher energy configurations of the elementary edge dislocation cores in the idealization of the liquid-like regions as distorted high angle grain boundaries. Since the initial state of the 2-D material before being melted consisted of a field of perfect hexagons subjected to periodic boundary conditions, certain conservation laws must apply to the defects in the disordered states of the material in the melt or below the melting temperature. These conservation laws were studied in considerable detail by Smith [17] in 2-D area filling polygons. In one limiting

form, where only 5, 6, and 7 sided polygons exist in the field, the numbers $P_n$ of the $n$ sided polygons relate to the numbers $C$ of the 4 edged corners by the conservation law of:

$$\sum_n (6-n)P_n - 2C = 0 \ . \tag{9}$$

Comparison of the three figures of Fig. 2a-2c shows that in the melt, the liquid-like material of the 5-7 sided polygon regions do not remain stationary in time, but are constantly shuffled, maintaining, however, a percolation condition on the average. Even so, percolating chains often break up and establish associations with other subsidiary chains, as apparently the quasi-ordered domains shift and rotate randomly. In this manner, the liquid-like material is capable of wandering over the cubic 2-D field, and can in principle have access to every point in the 2-D space. It is useful to consider this fluctuating disorder as a graphical representation of a configurational entropy $s_c$ attributable to the presence of the liquid-like material alone, which could be defined along conventional lines as:

$$s_c = k\ell n \left( \frac{(N/2)!}{((N/2)-n)!n!} \right) \ , \tag{10}$$

where $N$ is the total number of atoms in the cell, and $n$ is the number of the 5-7 sided pairs of polygons. The maximum in this configurational entropy occurs when $n = N/4$, or at a value of the fraction of the liquid-like material of 0.5. The actual fractions of liquid-like material made up of the 5-7 sided polygon pairs at the melting point was found to vary between a value of 0.36 to a high value of 0.41. On the basis of this, the configurational entropy is found to have reached 95% of its peak value given by the expression in Eqn. (10). Clearly, in the free energy of the liquid state, the internal potential energy of the atoms also plays an important role, and limits the role of the configurational entropy. This is manifested by the quasi-ordered regions which force the disordered liquid-like material into the border regions between the ordered regions. Nevertheless, the expression in Eqn. (10) furnishes a good guide to account for the overall fraction of the liquid-like material in the melt.

Examination of the break-up and re-formation of the percolating strings of the 5 and 7 sided polygons has shown that when such breaks occur through the transformation of these polygons into distorted hexagons, usually the "dissolved misfit" re-appears in the immediate neighborhood as a pair of new 5-7 sided polygons, associating themselves to the ends of other neighboring chains. This is to be expected in the crystal defect idealization, where terminations of chains of 5-7 sided polygons would represent terminations of high angle grain boundaries with a relatively high stress that would attract other 5-7 sided polygons to provide compensation of misfit. Alternatively, viewing the boundaries

of 5-7 sided polygons as high angle grain boundaries separating quasi-ordered domains, shifts in the domains will move the boundaries around, including directions where the geometrically necessary arrangement of dislocation cores requires occasional gaps between the 5-7 sided polygon dipoles.

In a more elementary form, gradual drifts of isolated 5-7 sided polygon dipoles towards each other, have also been observed occasionally. Such events, however, are quite rare, since isolated 5-7 sided polygon dipoles are themselves rare, at or around the melting point, where their combined glide and climb mobility could make a contribution to structural fluctuations.

Parenthetically, at low temperatures in well-relaxed structures of a high crystalline content, where such isolated 5-7 polygon pairs occasionally occur and stand out, their mobility is quite low. Nevertheless, in the structural relaxation process leading to material with increasing perfection through the disappearance of the liquid-like material, such pair-wise eliminations of 5-7 sided dipoles is topologically necessary, as we will demonstrate below. One such case of glide-controlled approach of two edge dislocations toward each other under their mutual attraction in a partially relaxed glass at $T^* = 0.1$ in the course of further relaxation is shown in the sequence of Fig. 3a-3e, in the upper right corner of the figures marked with arrows. The figure also shows clearly two metastable configurations in the slowly gliding edge dislocation as two adjoining polygons with 5 edges sharing a 4 edged corner. The dislocations are marked in Fig. 3a with the appropriate $T's$, to identify them and their mutual arrangement that should result in an attraction. Parenthetically, examinations of specific configurations in well-relaxed material at $T^* = 0.1$ have shown several instances where

an isolated edge dislocation has assumed the metastable configuration of two 5 sided adjacent polygons only to return to its initial configuration of a pair of 5-7 sided polygons. This indicates that the two neighboring 5-7 sided polygon configurations are the lower energy form and that the two 5 sided polygons indeed represent a metastable form of somewhat higher energy.

### *3.3 Structural Relaxation in the Subcooled Melt, $T_g < T < T_m$*

The sequence of structural relaxations at a temperature of $T^* = 0.2$ between $T_g$ and $T_m$ in the subcooled melt is shown in Figs. 4a-4d, starting at a time of 27 fluctuation periods, after initiation of the isothermal relaxation, Fig. 4a, and continuing to 100 fluctuation periods, Fig. 4d. Over this period of structural relaxation, it is evident that the overall content of the liquid-like material is decreasing monotonically, as it is expected to do. The overall fraction of liquid-like material in Fig. 4a, after 27 fluctuation periods has decreased from the starting fraction of about 0.4 in the melt to about 0.31. In this range, the percolating strings of liquid-like material are almost intact, up to a total relaxation period of 35. This is roughly the level of structural alterations studied in (I), where $T_g$ was established at a cooling rate involving a time period somewhat less than this relaxation time. In Fig. 4d, after a total relaxation time of 100 fluctuation periods, the total fraction of liquid-like material has decreased down to 0.19, and the percolation condition has clearly been broken, as the mutual misorientation between quasi-ordered domains has very markedly decreased. Thus, this end state of the material, associated with a slower rate of cooling, is now no longer

a subcooled liquid, but a well-relaxed glass. Apart from the gradual reduction of the liquid-like fraction of the material, the kinematics of the structural relaxation at $T^* = 0.2$, in the range of subcooled liquid, exhibit most of the modes of structural variations found in the high temperature melt.

### *3.4 Structural Relaxation below $T_g$, at $T^* = 0.1$*

Figures 5a-5e give a sequence of changes in the distribution of liquid-like material over a time of 200 fluctuation periods at $T^* = 0.1$. While at the beginning, in the as-quenched structure, a condition of near percolation exists, this disappears quite rapidly. Over the period of simulation, the fraction of the liquid-like material decreases monotonically from 0.33 to 0.049. Since the liquid-like material is made up of structural dipoles of 5-7 sided polygons, which should usually attract each other and result in cancellation when such pairs in exact compensating configurations encounter each other. This cancellation might be expected to obey second order kinetics, i.e.,

$$\frac{df}{dt} = -\alpha f^2 \ , \tag{11}$$

where $f$ is the fraction of liquid-like material, and $\alpha$ is primarily the reciprocal of a characteristic time constant. If this were indeed the case, a specific form of time dependent decrease should result, that should be:

$$1/f - 1/f_o = \alpha t \ . \qquad (12)$$

That this is indeed the case, is shown in Fig. 6. From the figure, we establish that the characteristic time constant $1/\alpha = 15$ fluctuation periods. This gives a first-order fit to the actually more complex and distributed kinetics of structural relaxation that will be the subject of a separate communication [13] (referred to earlier as (III)). Ahn and Li [18] have interpreted the kinetics of the strain recovery experiments of Berry [19] in $Pd_{80}Si_{20}$, with second order kinetics on the basis of an analog to cancellation of dislocation pairs. Our simulation is in agreement with their findings.

The steps in the elimination of liquid-like material are usually complex. Nevertheless, in the final stages of this elimination where a limiting idealization of such defects as edge dislocation cores in boundaries is useful, this point of view clarifies the kinetics of these processes considerably. Two examples of mutual cancellation of 5-7 sided polygon pairs that have been observed are shown in Fig. 7a and 7b. The pair in Fig. 7a acts like two slightly displaced opposite edge dislocations, which are not exactly on the same plane to cancel fully. The accompanying symbolic sketch below the polygons suggests that the two pairs attract to cancel. In the intermediate figure, they do not produce full cancellation, but result in a momentary partial interstitial, which in the last frame, is dispersed among the four hexagons by a small rearrangement of polygons. In

Fig. 7b, the two approaching dislocations have Burgers vectors making a 60° angle with each other, and are in a mutually attracting configuration. Upon contact, they react to give a single product dislocation with a Burgers vector making a 60° angle with both of the previous dislocations, as shown in the accompanying symbolic sketch. Clearly, the sequences of the relaxation shown in Figs. 5a-5e take the structure from a well-relaxed glass progressively to a crystal. On such a small simulation plane, the transition is gradual, and its onset cannot be clearly identified. This difficulty, however, is common in the study of atomic amorphous media, where no single threshold criterion has proved fully satisfactory.

The results of the structural relaxations at $T^* = 0.1$ over 200 fluctuation periods (4000 time steps) are typical of all structural relaxations, which we have studied and are most instructively viewed by comparing the changes in the distribution of a number of intensive local atomic properties, before and after the entire relaxation period. These results for the average atomic level enthalpy, Voronoi polygon volume (an indirect measure of free volume), site distortion parameter, atomic level pressure, atomic level maximum shear stress, and atomic level bulk modulus, are shown in Figs. 8-13, first as averages over all atoms (a), then for averages over only the softer $Cu$ atoms (b), and finally, for averages over only the stiffer $Zr$ atoms (c). In the figures, only the changes in the distributions have been shown that modify the initial distributions into the final distributions. In the cases of atomic levels of enthalpy, Voronoi polygon volume, and site distortion parameter, the extremes of excess properties have been markedly diminished to enrich the distributions at the low end. This is particularly clear

for the enthalpies and site distortion parameters, while in the case of the Voronoi polygon volume, both the large and the small VP volumes have been eliminated in favor of the intermediate volume VPs, i.e., the hexagons. There are significant differences between the $Zr$ atom with its stiffer environment, and the $Cu$ atom with its softer environment. The structural misfit produced by the disorder is more readily accommodated by the softer $Cu$ atoms, as would be expected from the analogous case of a random network of interconnected stiff and compliant springs. In such a network with incorporated random misfit, more energy is stored in the more compliant springs than in the stiffer springs, i.e., in the $Cu$ sites, rather than in the $Zr$ sites. Thus, upon structural relaxation, the changes in excess enthalpy are larger for the $Cu$ sites. Equally dramatic differences are apparent in the changing atomic level pressure distributions between the $Cu$ and the $Zr$ sites. Evidently, in the initial highly disordered glassy state, the stiffer and larger $Zr$ atoms form an interconnected super structure in compression with the interspersed $Cu$ atoms being generally under negative pressure. The additional applied pressure in the simulation is also largely born by the $Zr$ super structure. Upon structural relaxation, steadily better fits among the atoms are achieved, no doubt because of an increasing chemical short range order, as has been already reported by Kabayashi and Takeuchi [10]. As a result, the $Cu$ atoms are subjected to less negative pressure, and the $Zr$ atoms are subjected to less positive pressure. Hence, the incremental atomic level pressure is positive on the $Cu$ atoms, and negative on the $Zr$ atoms. The decrease of the negative pressure from the $Cu$ atoms is also evident from an increase in their bulk modulus.

## IV. DISCUSSION

### *4.1 Characteristics of the 5 and 7 sided Polygon Pairs*

In (I), we have demonstrated that in a distorted field of area filling polygons, the average heptagons have a 10% larger area than the average hexagons, while the average pentagons are only 3% smaller than the latter – making the pair of pentagon and heptagon, i.e., the 5-7 pair, have an excess area of 7% over two average hexagons. Considering that the average hexagon at the melting point itself has an average area that is about 9% larger than its area of $0^{o}K$, the 5-7 sided pair of polygons are 16% larger than two reference hexagons at rest. Such an areal expansion should produce significant loss of cohesion in any realistic inter-atomic binding potential and therefore, constitutes an element of liquid-like material. In the polygon mats of molten material, occasional octagons and squares were also found. These, however, were always part of the string of liquid-like material, and were interpreted as further distortions of 7 sided and 5 sided polygons.

Since the 5-7 sided polygon pairs were found to hold the key to many structural and mechanical relaxation phenomena, some of their other properties were also evaluated. In Fig. 14a, the change in the site distortion parameter is shown with the changing number of edges of polygons in a simulation at $T^{*} = 0.1$. The solid line gives the change in the raw measure of the site distortion, as obtained from an evaluation of Eqn. (7). If corrections are made according to Eqn. (8), however, subtracting the trivial decrease in the distortion parameter with

increasing numbers of sides of polygons given in Table I, the information shown by the broken lines in Fig. 14a is obtained, which indicates that the average pair of hexagons are far less distorted than a 5-7 pair of polygons. The corresponding evaluation for the average excess enthalpy of polygons over that for the average hexagon, as evaluated by Eqn. (6), is shown in Fig. 14b. Thus it is clear that the excess free volume in the 5-7 sided polygon pairs results in excess enthalpy.

### *4.2 Topological Features of Structural Relaxation*

The surprising aspect of the two-dimensional simulation of structural fluctuations in the melt and the features of its relaxations below the melting point are the striking parallels that it has revealed to a defective crystalline material. In our simulation, a melt is made up of very small quasi-ordered domains of more or less distorted hexagons separated by boundaries of much more severely distorted polygons, which are analogous to high angle grain boundaries. This distorted boundary material was found to be predominantly made up of pairs of polygons with 5 and 7 sides arranged mostly in....5-7-5-7.... sequences, with occasional breaks bridged by a severely distorted hexagon. In the melt, this boundary material was found to occupy about 40% of the total area. Since the boundary material is on the average one atom thick, the quasi-ordered domains that it separates are only 3-5 atoms across. Thus, the quasi-ordered domains should not be viewed as individual grains, but at best, only as topologically short range ordered material. Since the polygon pairs with 5 and 7 sides represent edge dislocations in a perfect mat, the boundary material where they

are sequentially arranged must be viewed in abstraction as a high angle grain boundary made up entirely of dislocation cores, having collectively no long range stress field characteristic of dislocations. In fact, the only dominant property of the boundary material with the 5 and 7 sided polygons is an excess volume (free volume) of about 7% larger than the average volume of the distorted hexagons in the quasi-ordered domains, which themselves are about 9% larger at the melting point than the reference hexagons of a perfect mat at $0°K$. Thus, the boundary material has an average dilatation of about 16% in comparison with a perfect mat at $0°K$. This should reduce the inter-atomic cohesion in the boundaries to a relatively low level. Following Cohen and Grest [20], we have called the boundary material "liquid-like", and have noted that it percolates through the entire 2-D space. That this material is indeed liquid-like, and that it prescribes the sites for shear transformations when the mats are sheared, is presented and discussed in great detail in the last of the accompanying communications, which we will refer to as IV [21].

Occasional edge dislocations are also found in quasi-ordered domains which have shown mutual attractions to each other, have moved by glide, and in a few instances, fused with other dislocations to give cancellation of pairs or expected reaction products. Such events, however, where isolated well-delineated dislocations have given purely dislocation related glide, and associated phenomena were quite rare. Nevertheless, in the structural relaxations, increasing order and decreasing misorientation in the quasi-ordered domains through the elimination of the 5-7 sided pairs of polygons as dislocation cores in the boundary material, could only have happened by pair-wise cancellations of the 5-7 sided

polygon pairs. The reasonably good fit to second order kinetics of the reduction of the fraction of boundary material is in support of this sequence of events.

The results of our simulation are in remarkable agreement with the observations of Fukushima and Ookawa [22], who carried out quite detailed pioneering experiments on meiting with vibrating Bragg soap bubble rafts. They reported that in their rafts, melting occurred when a high concentration of high angle grain boundaries divided the raft up into small isolated quasi-crystalline domains of roughly the same dimensions as our quasi-crystalline domains. Since the inter-bubble potential provides a good match to interatomic pair potentials for close-packed metal atoms in the binding region (for a comparison of the potentials, see Shi and Argon [23]) their findings should not be surprising – even though the vibrational amplitudes of bubbles must have had a substantial component out of the plane of the raft.

### *4.3 Generalization of Results to Three Dimensions*

Clearly, the results of our simulation must be taken with some caution. As already mentioned in (I), two-dimensional disordered media entraps larger free volume than three-dimensional matter – if the disorder were indeed uniformly spread out. It can be argued, however, that the partitioning of order and disorder could not be much different in three-dimensional amorphous media. Certainly, the make up of the percolating liquid-like boundary surfaces in three-dimensional material will have a larger collection of polyhedra that provides a transition between the different quasi-lattices of the small ordered domains.

Self-consistent model studies of packing of rigid spheres randomly in 3-D spaces have indicated that the mechanical properties of the medium assume rigid behavior when a percolation criterion is reached at a volume fraction of 0.4 [24,25], which is almost identical to the value for the liquid-like material boundaries in our complementary case of 2-D simulation, where this fraction of material is deformable. Although the spatial arrangement of the quasi-ordered regions in 3-D space cannot be determined from these studies, it is quite likely that they are equiaxed domains leaving behind walls of a closed-cell network or liquid-like material, rather than being arranged in a spoke network. Thus, we expect that most of the qualitative observations from our 2-D simulation should be applicable to 3-D materials, particularly on topological features and on the inelastic mechanical response. The latter will be the subject of our last communication (IV) [21].

## ACKNOWLEDGEMENT

The research reported here has received support from a number of different sources. In the early phases, the computations were made possible by a small seed grant from the NSF/MRL Grant DMR-84-18718, through the Center for Materials Science and Engineering at M.I.T. In later phases, support for it was derived from an NSF Grant No. DMR-85-17224 and from an Advanced Research Projects Agency Contract No. N00014-86-K-0768. Partial salary support to DD came from a Fellowship from the Allied Corporation of Morristown, NJ, for which we are grateful to Dr. Lance Davis.

## REFERENCES


1. Y. Waseda, T. Masumoto, and S. Tomizawa, Can. Met. Quart., 16, 143 (1977).
2. H.S. Chen, Reports on Progress in Physics, 43, 353 (1980).
3. N. Morito and T. Egami, Acta Met., 32, 603 (1984).
4. D. Deng and A.S. Argon, Acta Met., 34, 2011 (1986).
5. D. Deng and A.S. Argon, Acta Met., 34, 2025 (1986).
6. F. Spaepen and A.I. Taub, in "Amorphous Metallic Alloys", edited by F.E. Luborsky (Butterworths: London), p. 231 (1983).
7. R.L. Freed and J.B. Vander Sande, Acta Met., 28, 103 (1980).
8. L.C.E. Struik, "Physical Aging in Amorphous Polymers and other Materials" (Elsevier: Amsterdam) (1978).
9. S. Takeuchi, K. Maeda, and S. Kobayashi, in "Amorphous Materials: Modeling of Structure and Properties", edited by V. Vitek (AIME: New York), p. 305 (1983).
10. S. Kobayashi and S. Takeuchi, J. Phys: Met. Phys., 14, 23 (1984).
11. S. Kobayashi, K. Maeda, and S. Takeuchi, Acta Met., 28, 1641 (1980).
12. D. Deng, A.S. Argon, and S. Yip, (I), submitted to Acta Met..
13. D. Deng, A.S. Argon, and S. Yip, (III), submitted to Acta Met..

14. T. Egami and V. Vitek, in "Amorphous Materials: Modeling of Structure and Properties", edited by V. Vitek (AIME: New York), p. 127 (1983).

15. M. Born and K. Huang, "Dynamical Theory of Crystal Lattices" (Clarendon Press: Oxford) (1954).

16. K. Maeda and S. Takeuchi, Phil. Mag., 44, 643 (1981).

17. C.S. Smith, "A Search for Structure" (M.I.T. Press: Cambridge, Mass.), Second Printing, p. 16 (1982).

18. T.M. Ahn and J.C.M. Li, Scripta Met., 14, 1057 (1980).

19. B.S. Berry, in "Metallic Glasses" (ASM: Metals Park, Ohio), p. 224 (1978).

20. M.H. Cohen and G.S. Grest, Phys. Rev., (B), 20, 1077 (1979).

21. D. Deng, A.S. Argon, and S. Yip, (IV), submitted to Acta Met..

22. E. Fukushima and A. Ookawa, J. Phys. Soc. Japan, 10, 970 (1955).

23. L.-T. Shi and A.S. Argon, Phil. Mag., A46, 255 (1982).

24. J.W. Hutchinson, Proc. Roy. Soc. (London), A319, 247 (1970).

25. I.-W. Chen and A.S. Argon, Acta Met., 27, 785 (1979).

## TABLE I

Base Levels of Distortion Parameter $w_o$ for regular Polygons

| Polygon | $w_o$ |
|---|---|
| Equilateral triangle | 1.286 |
| Square | 1.128 |
| Pentagon | 1.075 |
| Hexagon | 1.050 |
| Heptagon | 1.036 |
| Octagon | 1.027 |

## FIGURE CAPTIONS

Fig. 1 Schematic representation of quenching history in the structural relaxation simulations: ABCD heating path leading to melting and superheating, DE slow cooling in equilibrium, EF cooling at infinite rate, and FG isothermal structural relaxation.

Fig. 2 Structural fluctuations in a high temperature melt at $T^* = 0.3$ ($= 1.2\ T_m$): (a) after 15 fluctuation periods $\eta$ (b) after 20 fluctuations, (c) after 25 fluctuations. Note the distribution of liquid-like material made up of 5-7 sided polygon pairs.

Fig. 3 A sequence of glide-like approach of two edge dislocations in a quasi-ordered domain at $T^* = 0.1$. The position and nature of dislocations are indicated with arrows and letters $T$ in frame (a). Frames b-e show continued stages of approach.

Fig. 4 Structural relaxation sequences in a subcooled melt at $T^* = 0.2$ ($T_g < T < T_m$): (a) after $t = 27\eta$, (b) $t = 30\eta$, (c) $t = 35\eta$, and (d) $t = 100\eta$, showing progressive loss of liquid-like material.

Fig. 5 Structural relaxation sequences in a glass at $T^* = 0.1$ ($T < T_g$): (a) $t = 0$, (b) $t = 20\eta$, (c) $t = 70\eta$, (d)$t = 120\eta$, and (e) $t = 200\eta$.

Fig. 6 Time dependent reduction in fraction of liquid-like material at $T^* = 0.1$ during monotonic structural relaxation. The relationship

indicates second order kinetics arising from pair-wise cancellation of polygon dipoles.

Fig. 7 Two sequences of cancellation of dipoles: (a) dipole cancellation analogous to two opposite edge dislocation cores, (b) dipole reduction analogous to reaction of two 60° edge dislocation cores.

Fig. 8 Total incremental effect of structural relaxation at $T^* = 0.1$ on atomic level enthalpy: (a) all atoms, (b) $Cu$ atoms only, and (c) $Zr$ atoms only.

Fig. 9 Total incremental effect of structural relaxation at $T^* = 0.1$ on volume per atom (Voronoi polygon volume): (a) all atoms, (b) $Cu$ atoms only, and (c) $Zr$ atoms only.

Fig. 10 Total incremental effect of structural relaxation at $T^* = 0.1$ on atomic site distortion parameter: (a) all atoms, (b) $Cu$ atoms only, and (c) $Zr$ atoms only.

Fig. 11 Total incremental effect of structural relaxation at $T^* = 0.1$ on atomic level pressure: (a) all atoms, (b) $Cu$ atoms only, and (c) $Zr$ atoms only.

Fig. 12 Total incremental effect of structural relaxation at $T^* = 0.1$ on atomic level maximum shear stress: (a) all atoms, (b) $Cu$ atoms only, and (c) $Zr$ atoms only.

Fig. 13 Total incremental effect of structural relaxation at $T^* = 0.1$ on atomic level bulk modulus: (a) all atoms, (b) $Cu$ atoms only, and (c) $Zr$ atoms only.

Fig. 14 Comparison of intensive properties of polygons with six, five, and seven sides for partially relaxed mats at $T^* = 0.1$: (a) corrected distortion parameter for average hexagon is less than those for average pentagon and heptagon, (b) atomic level enthalpy is lower for hexagons than for pentagons and heptagons.

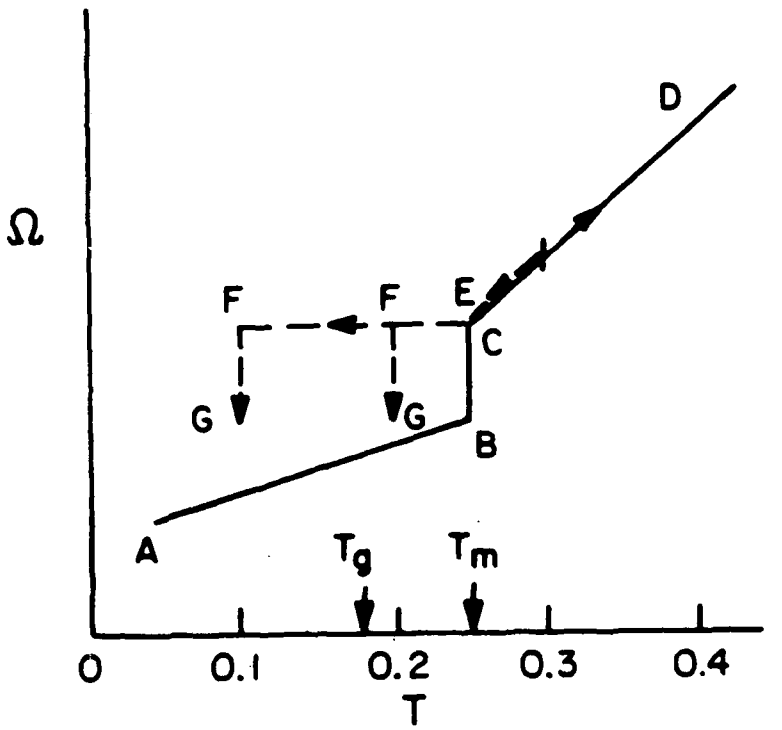


Fig. 1 - Schematic representation of quenching history in the structural relaxation simulations: ABCD heating path leading to melting and superheating, DE slow cooling in equilibrium, EF cooling at infinite rate, and FG isothermal structural relaxation.

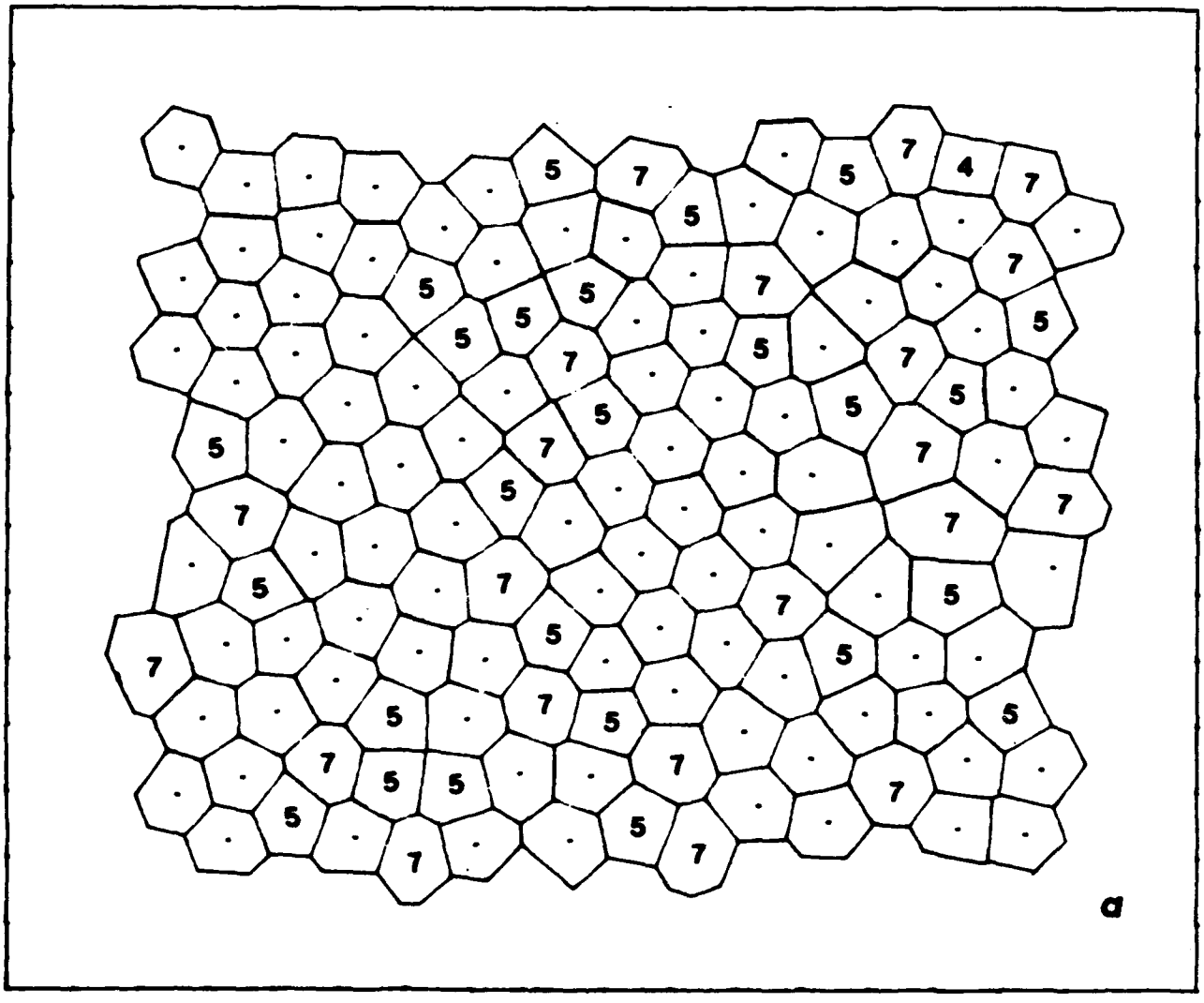


Fig. 2 - Structural fluctuations in a superheated melt at $T^* = 0.3$ ($= 1.2\ T_m$): (a) after 15 fluctuation periods $\tau$, (b) after 20 fluctuations, (c) after 25 fluctuations. Note the distribution of liquid-like material made up of 5-7 sided polygon pairs.

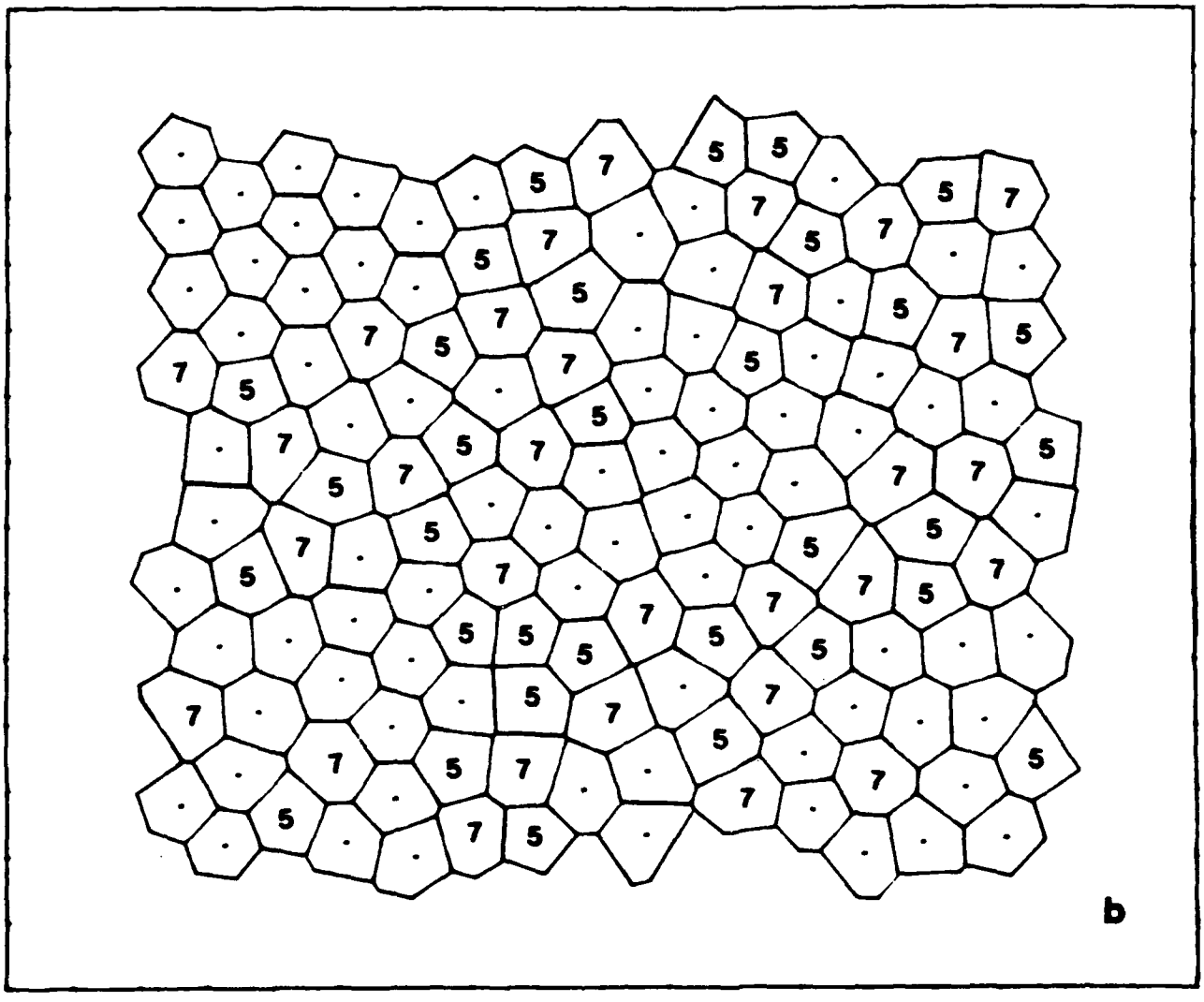


Fig. 2b

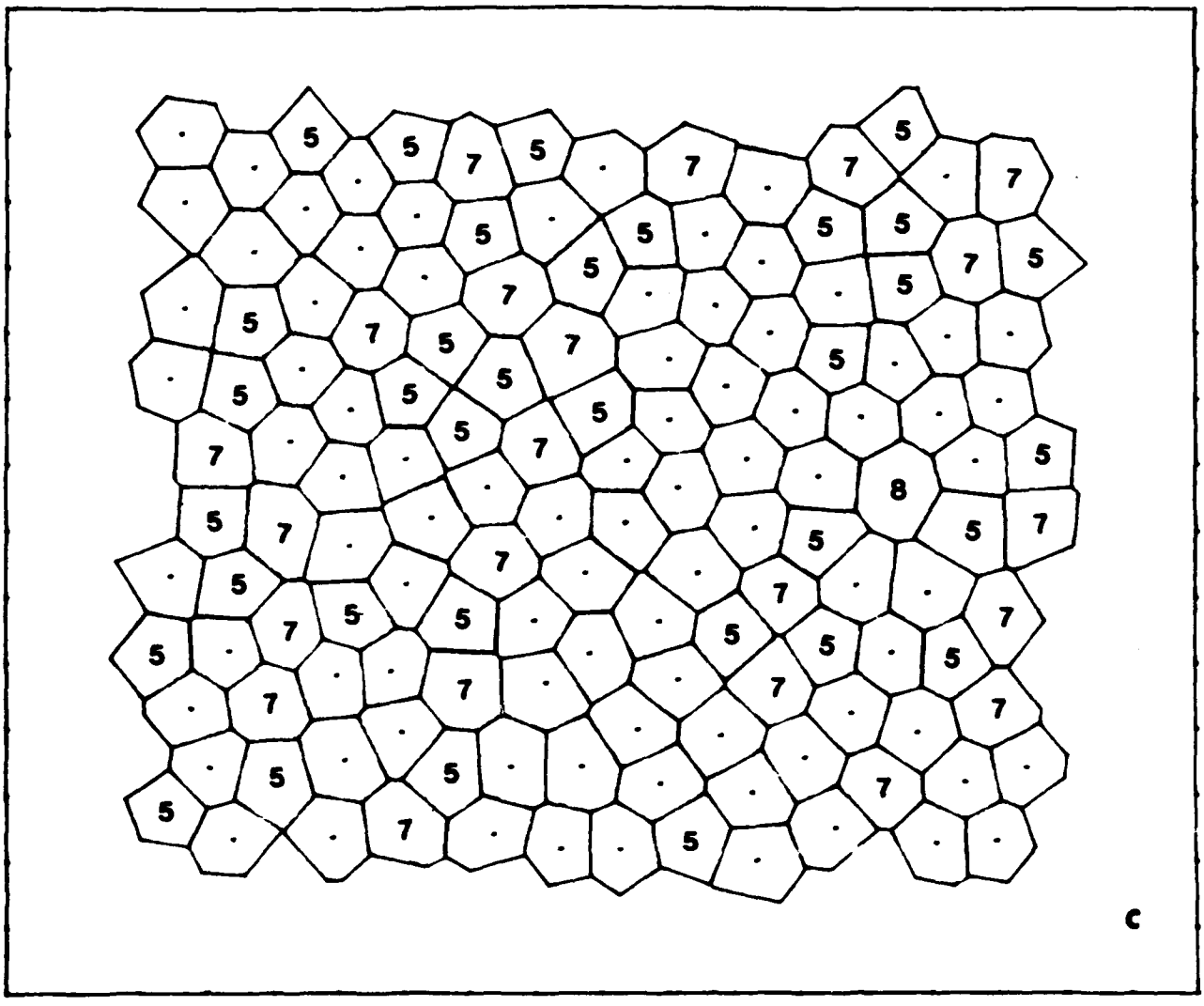


Fig. 2c

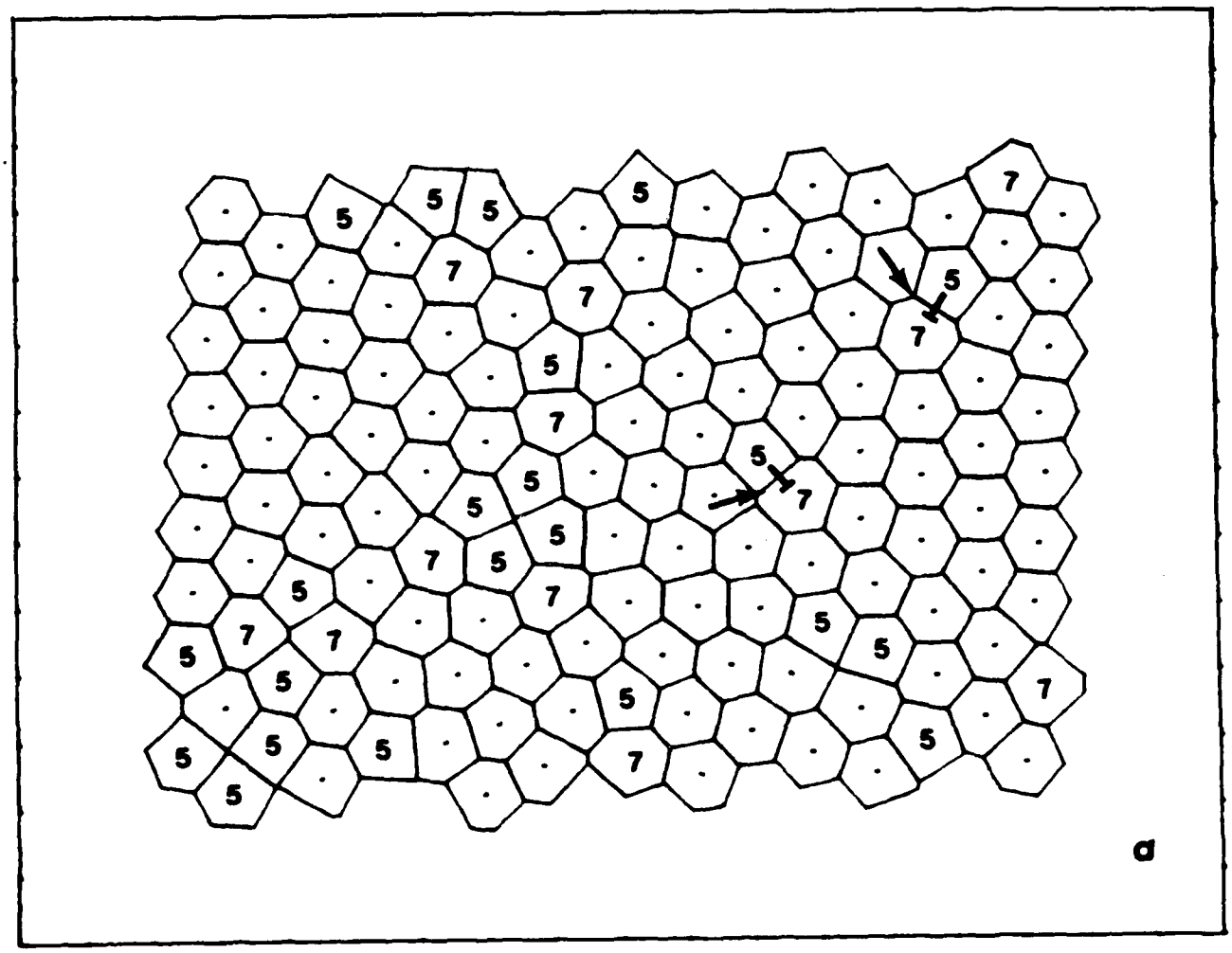


Fig. 3 - A sequence of glide-like approach of two edge dislocations in a quasi-ordered domain at $T^* = 0.1$. The position and nature of dislocations are indicated with arrows and letters T in frame (a). Frames b-e show continued stages of approach.

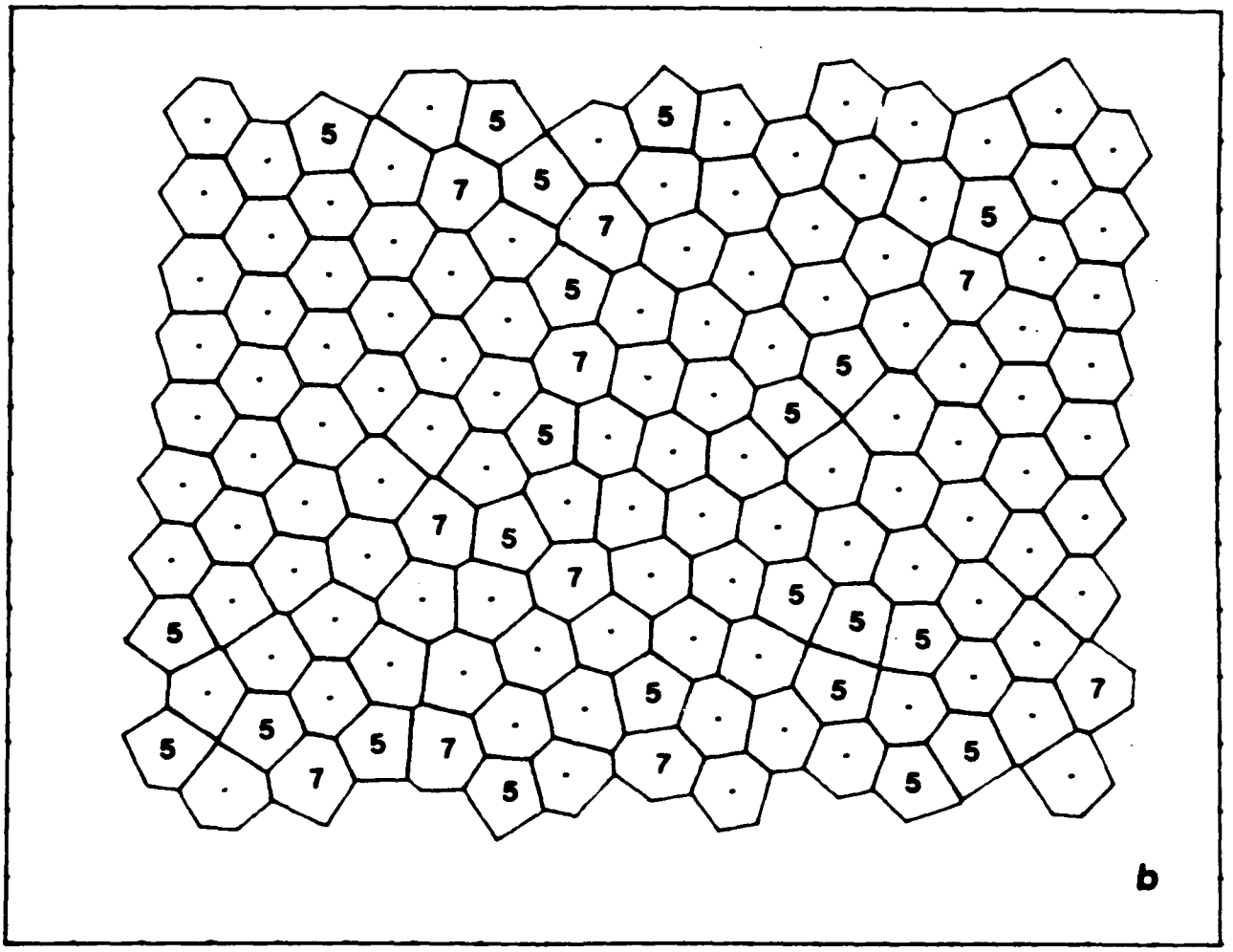


Fig. 3b

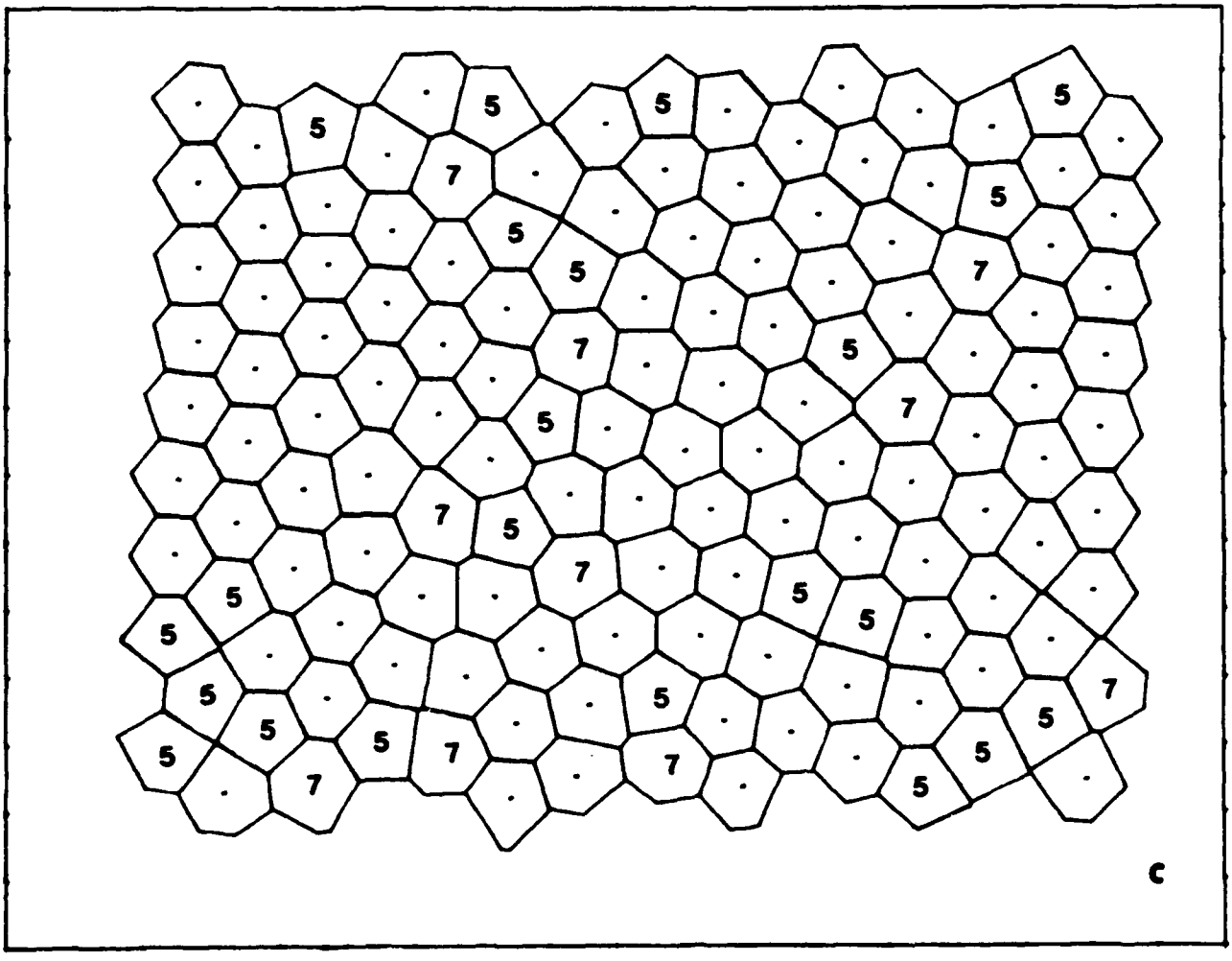


Fig. 3c

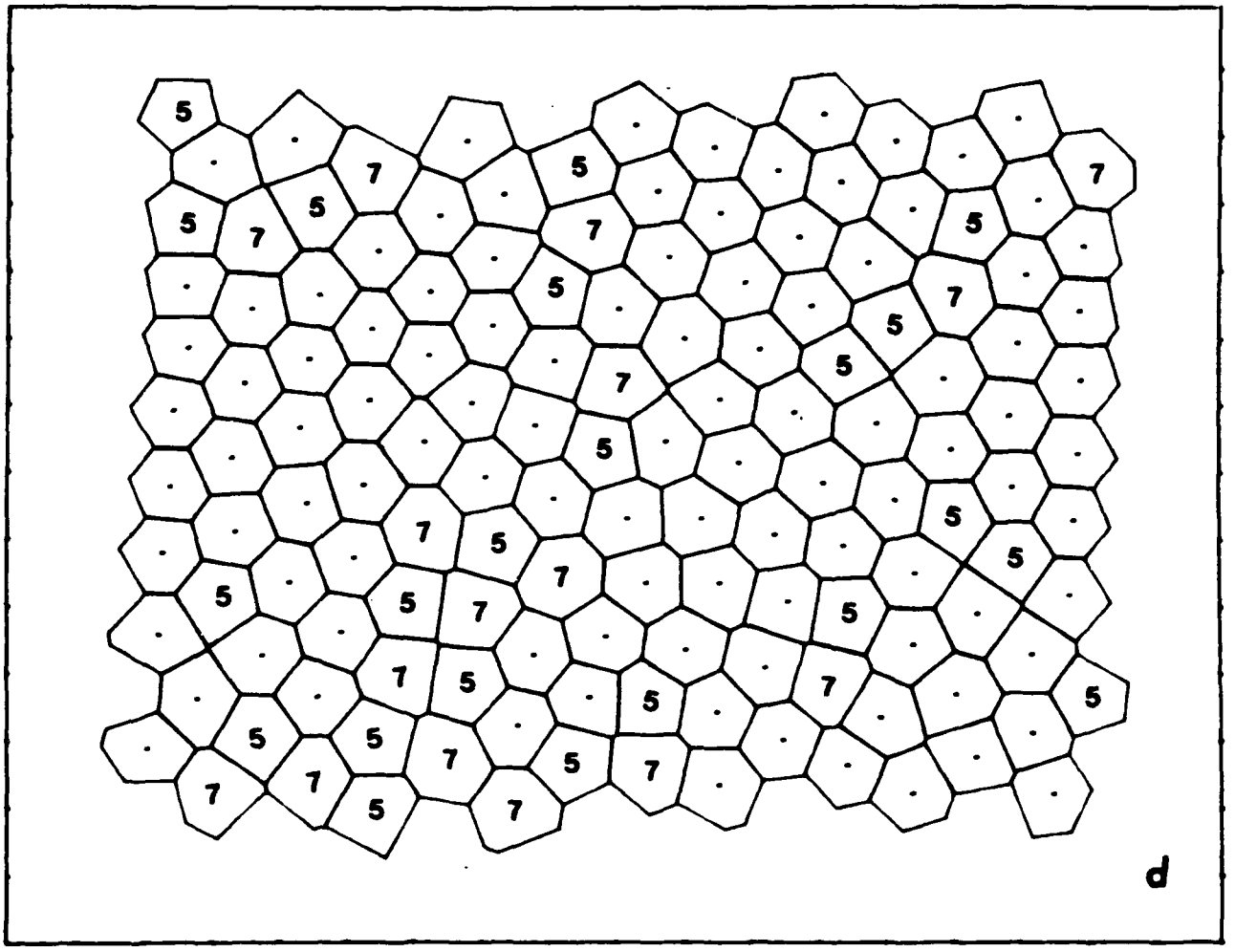


Fig. 3d

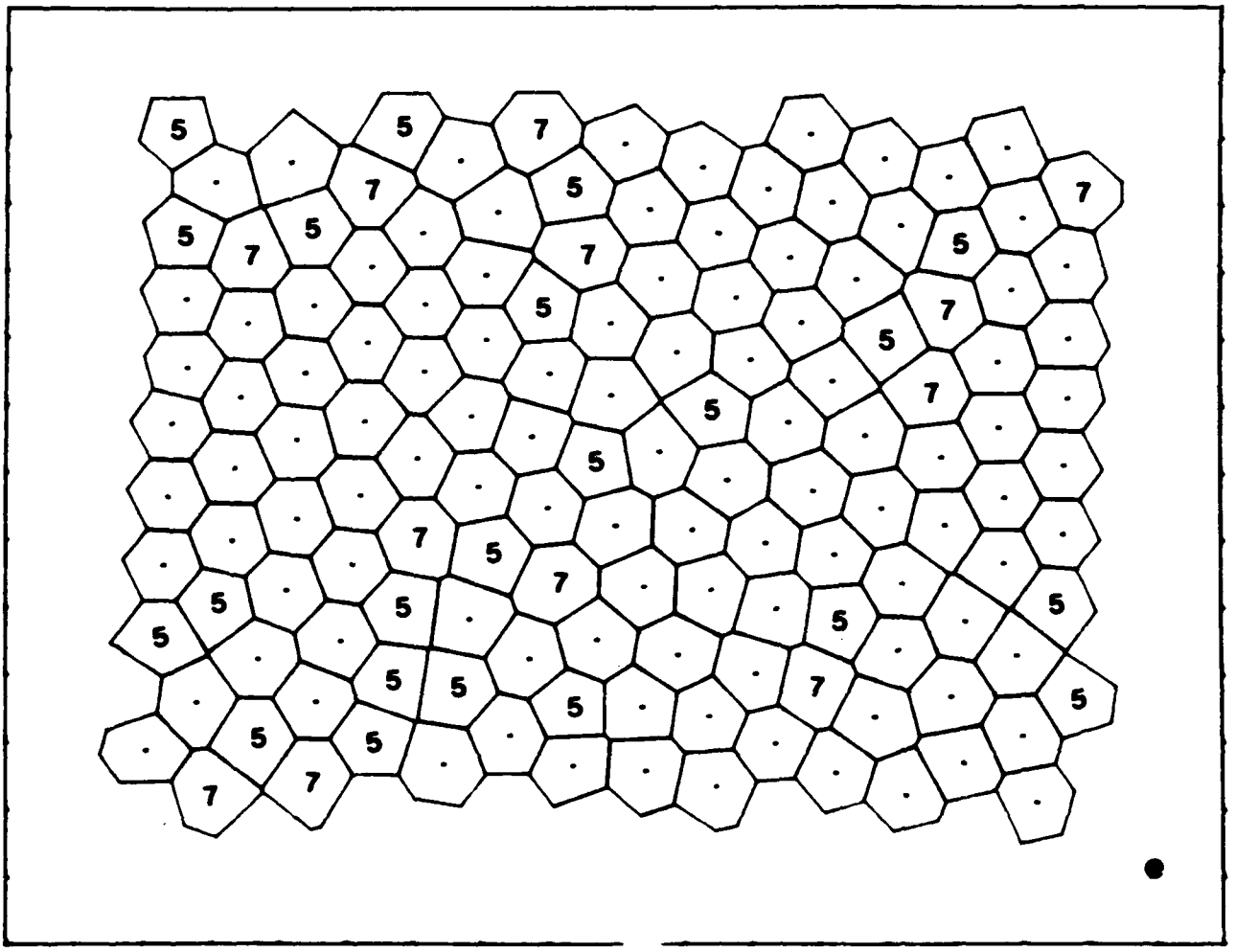


Fig. 3e

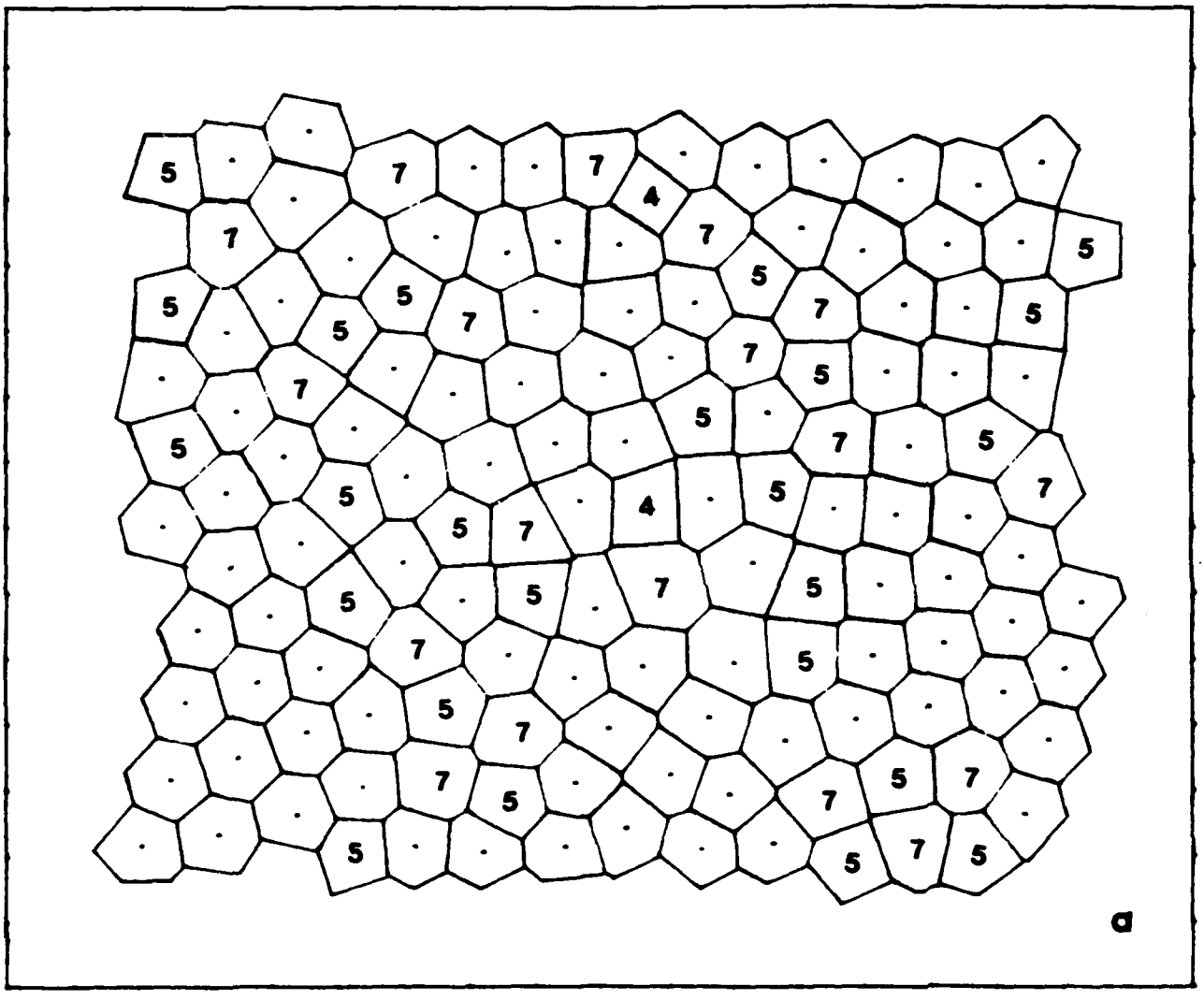


Fig. 4 - Structural relaxation sequences in a subcooled melt at $T^* = 0.2$ ($T_g < T < T_m$): (a) after $t = 27\tau$, (b) $t = 30\tau$, (c) $t = 35\tau$, and (d) $t = 100\tau$, showing progressive loss of liquid-like material.

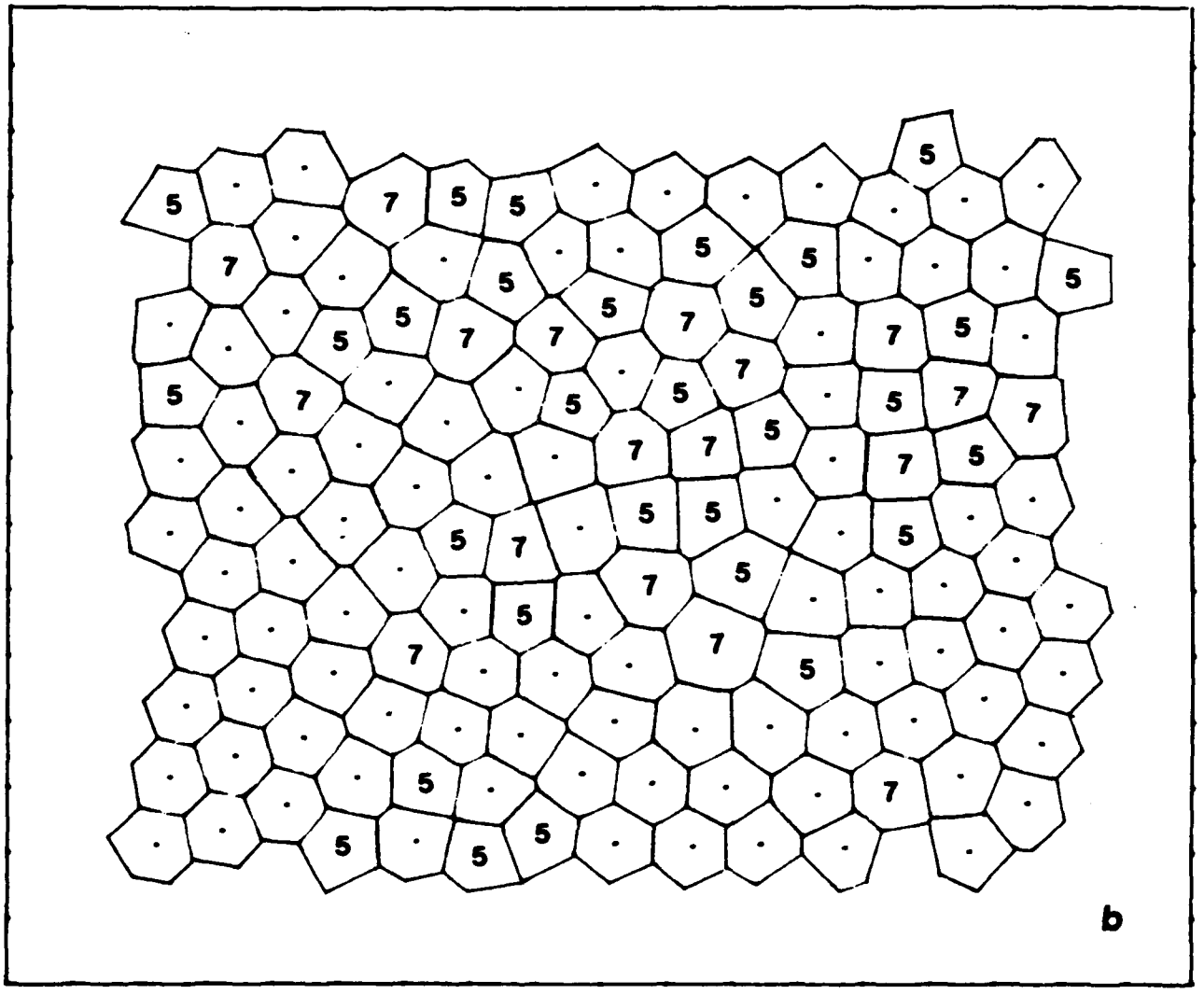


Fig. 4b

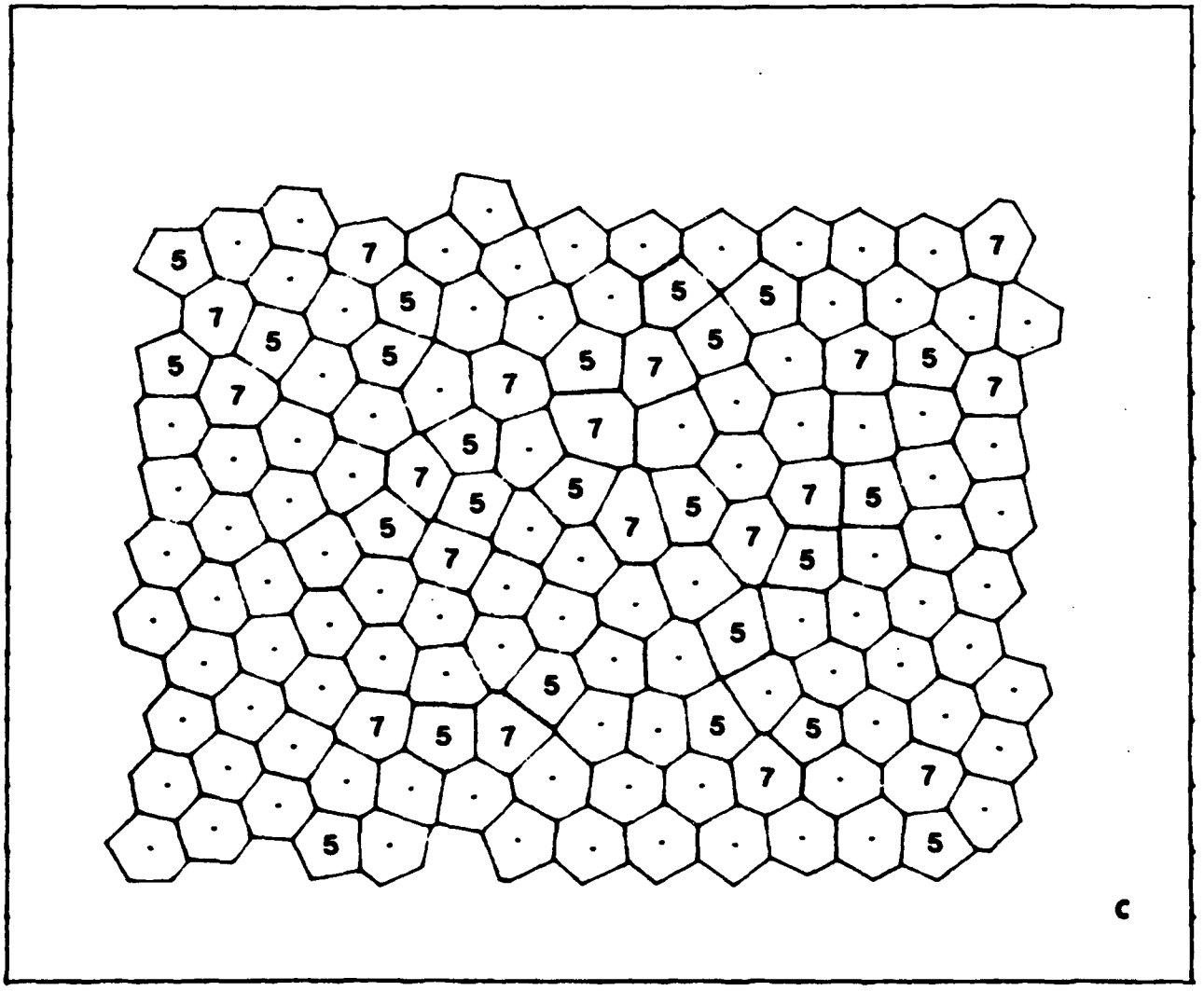


Fig. 4c

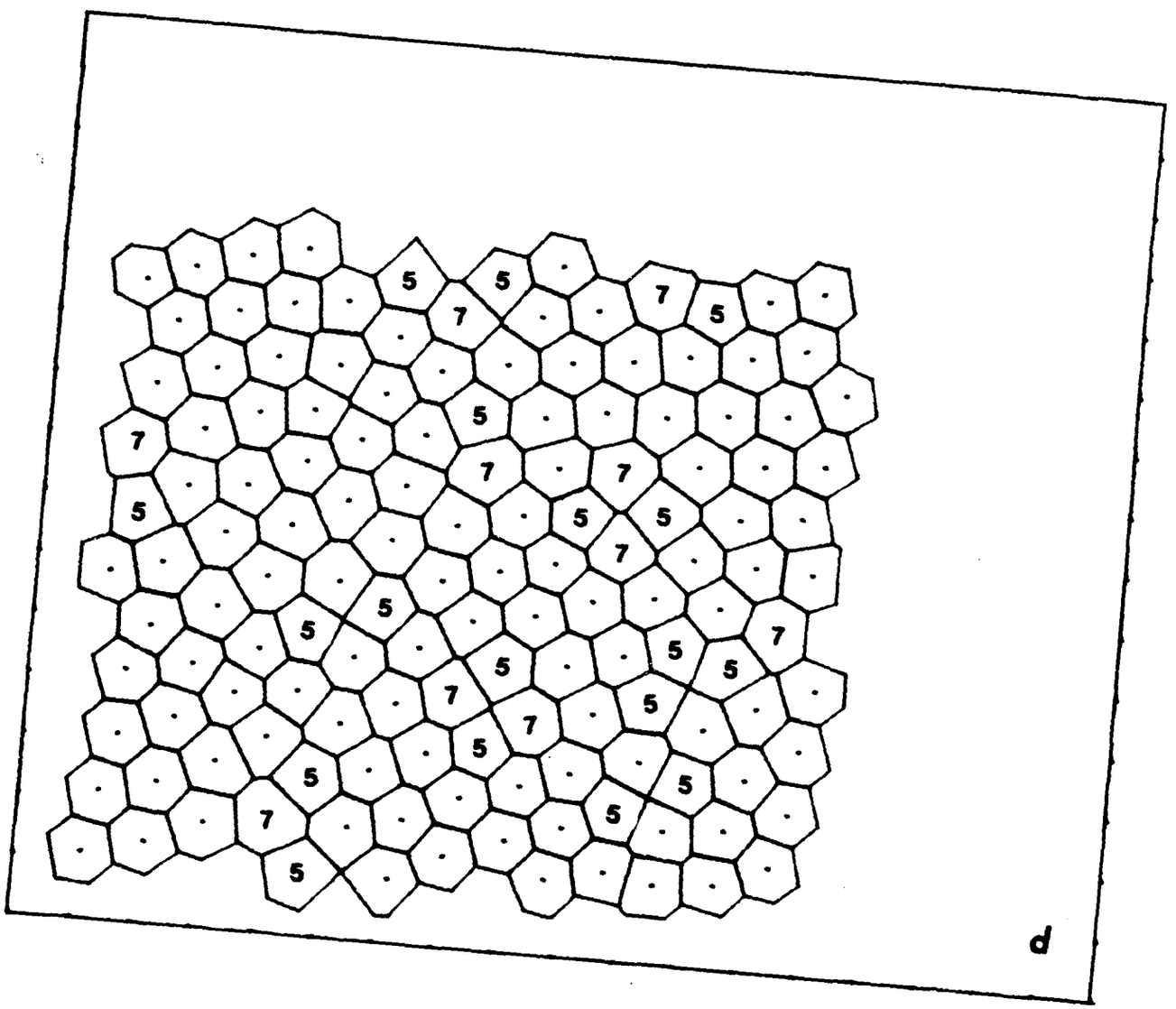


Fig. 4d

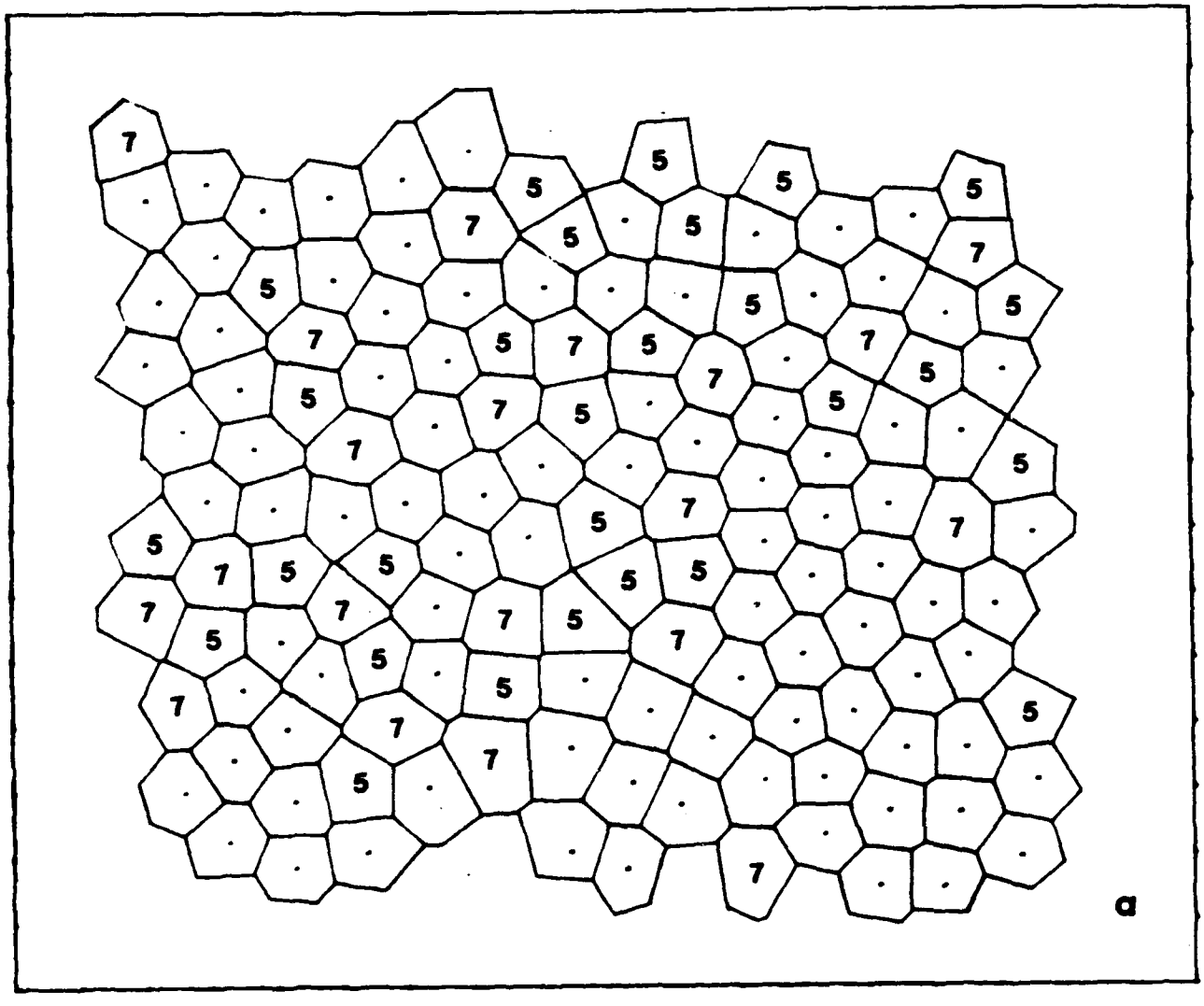


Fig. 5 - Structural relaxation sequences in a glass at $T^* = 0.1$ ($T < T_g$): (a) $t = 0$, (b) $t = 20\tau$, (c) $t = 70\tau$, (d) $t = 120\tau$, and (e) $t = 200\tau$.

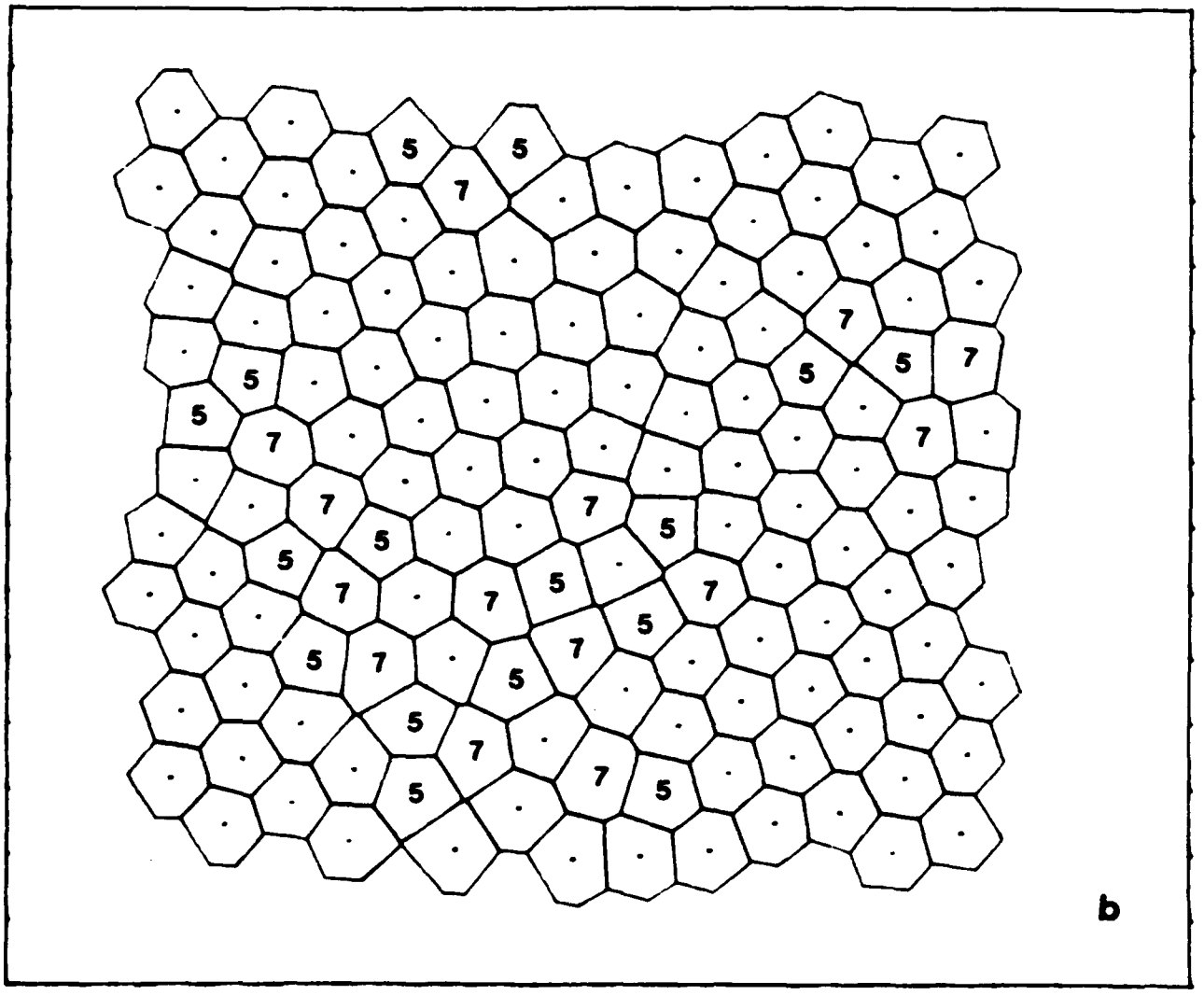


Fig. 5b

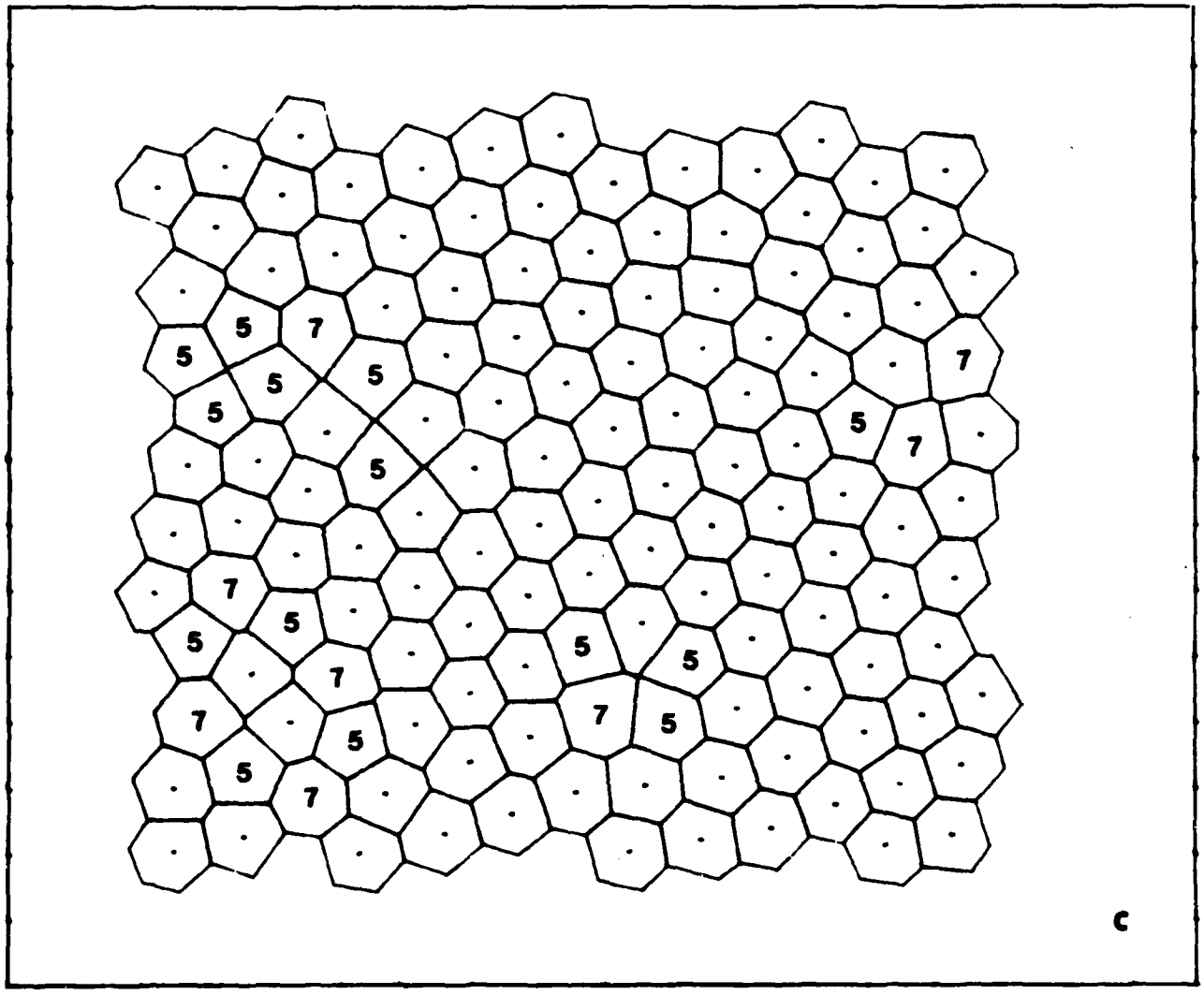


Fig. 5c

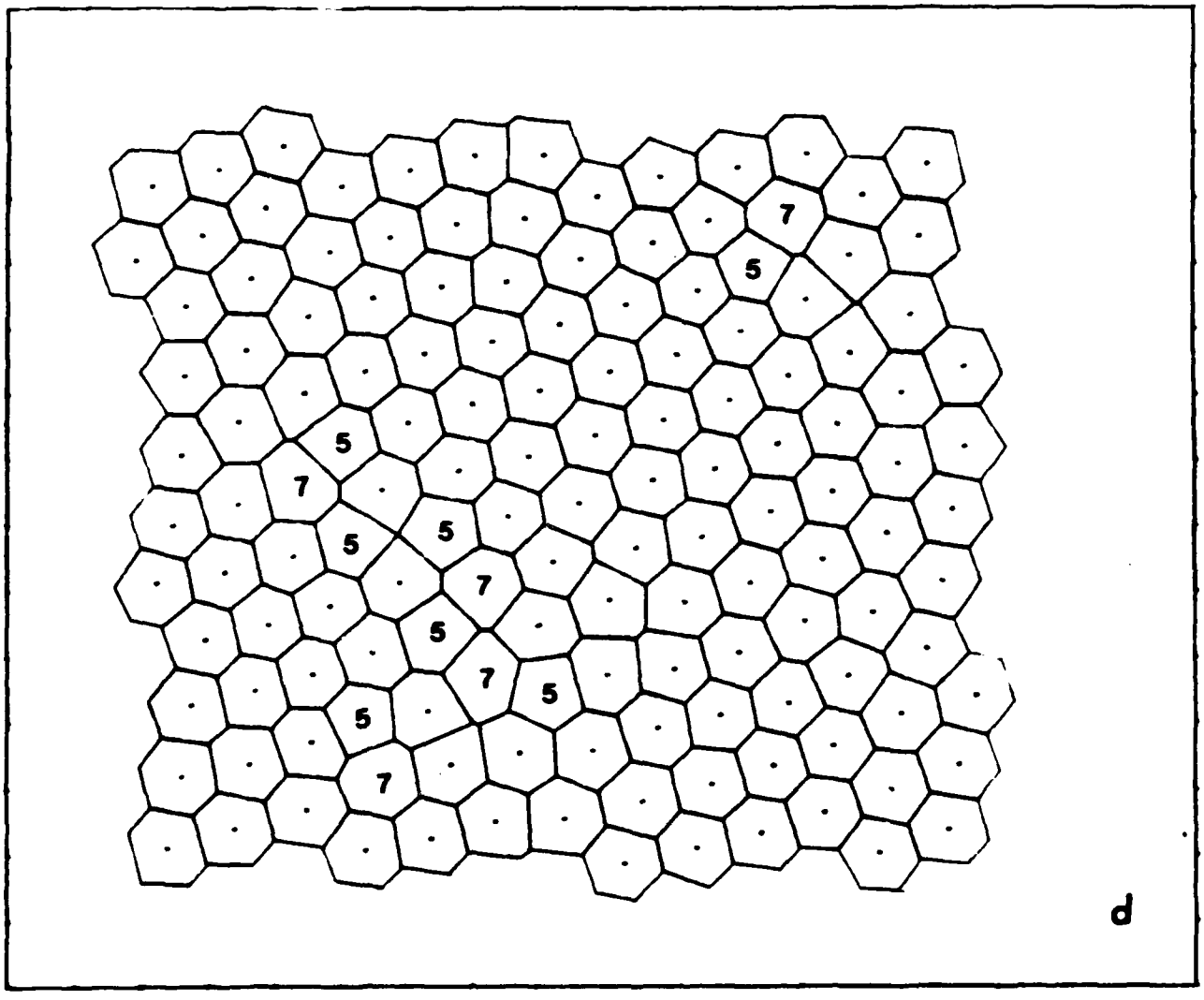


Fig. 5d

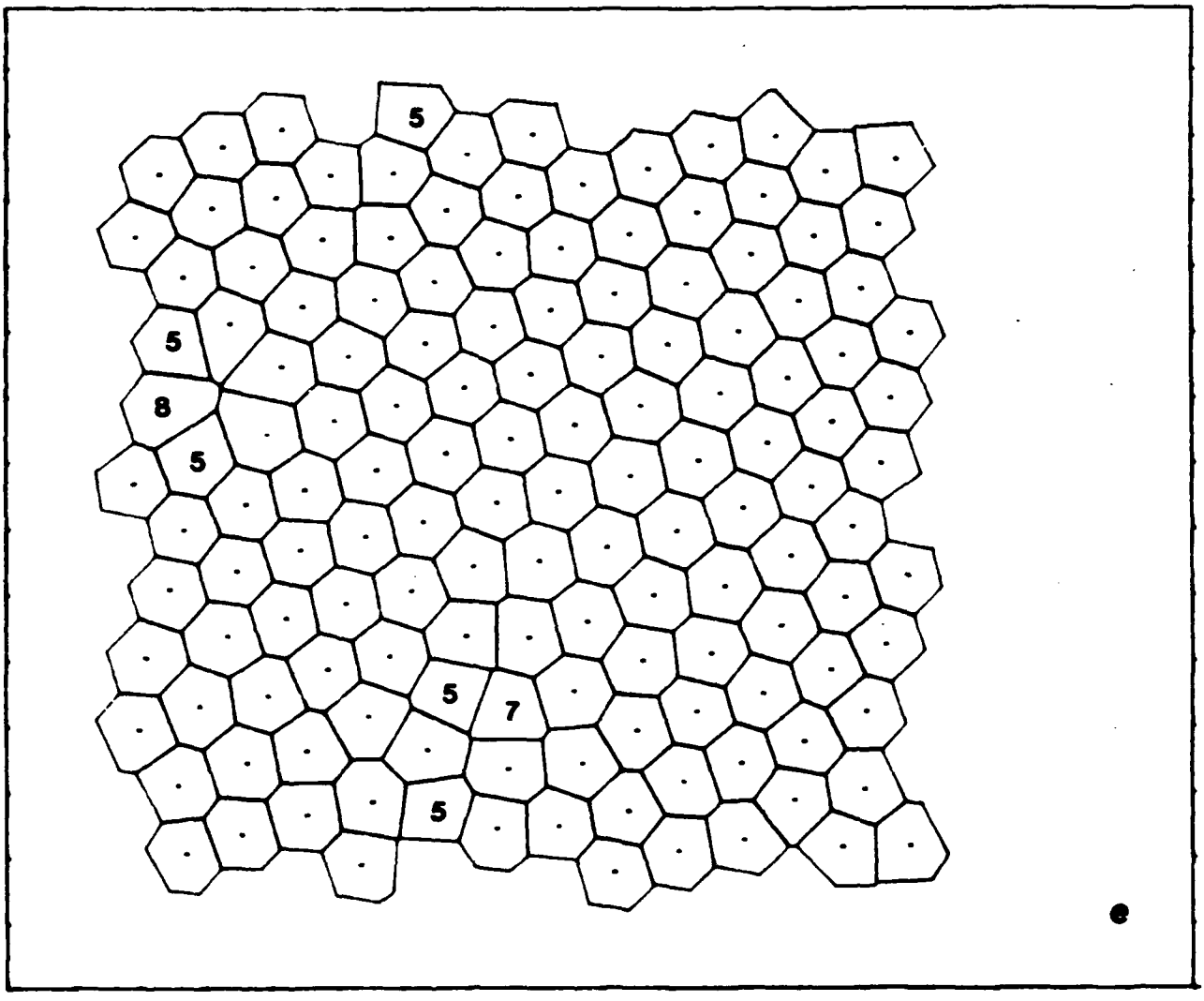


Fig. 5e

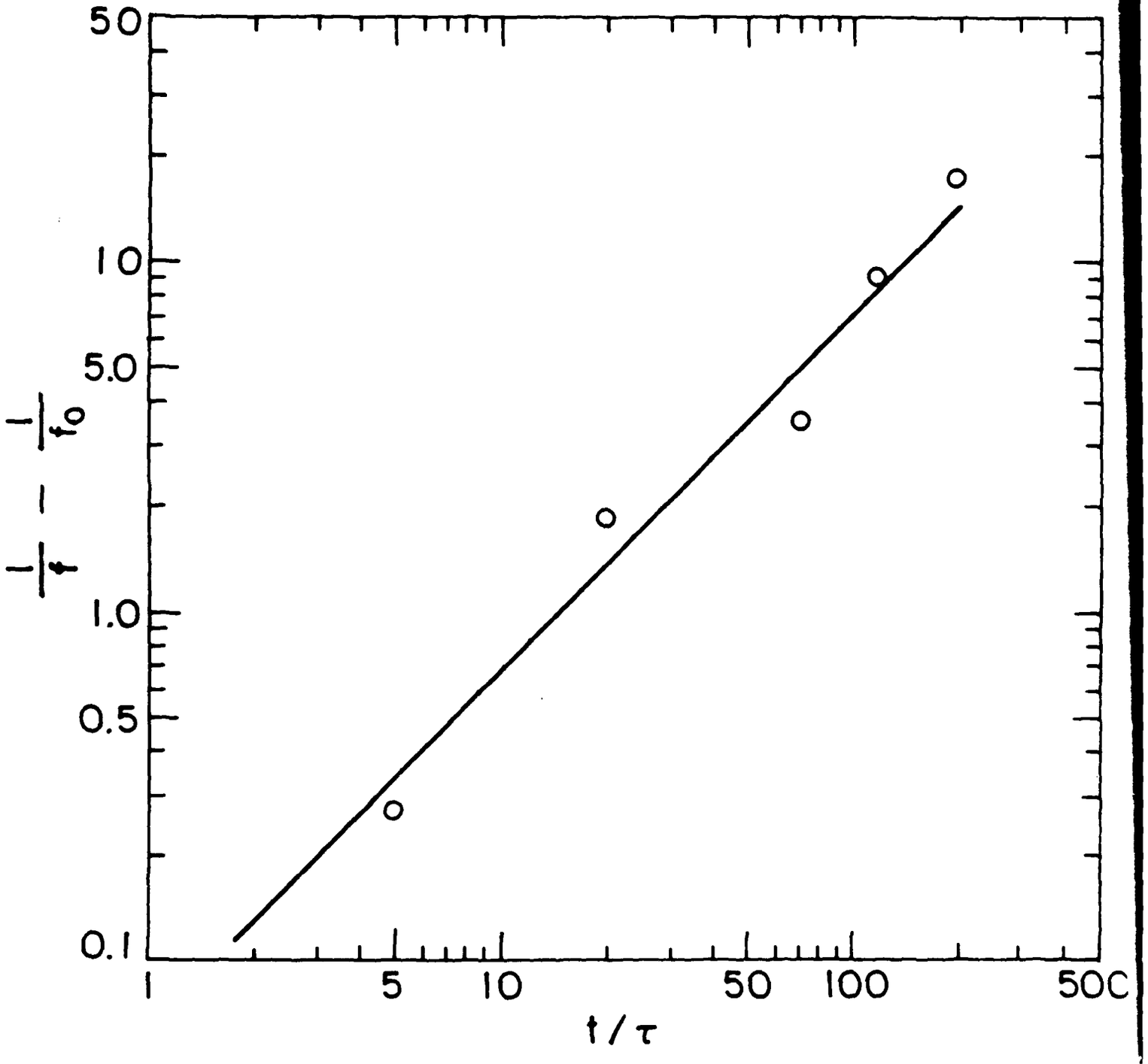


Fig. 6 - Time dependent reduction in fraction of liquid-like material at $T = 0.1$ during monotonic structural relaxation. The relationship indicates second order kinetics arising from pair-wise cancelletion of polygon dipoles.

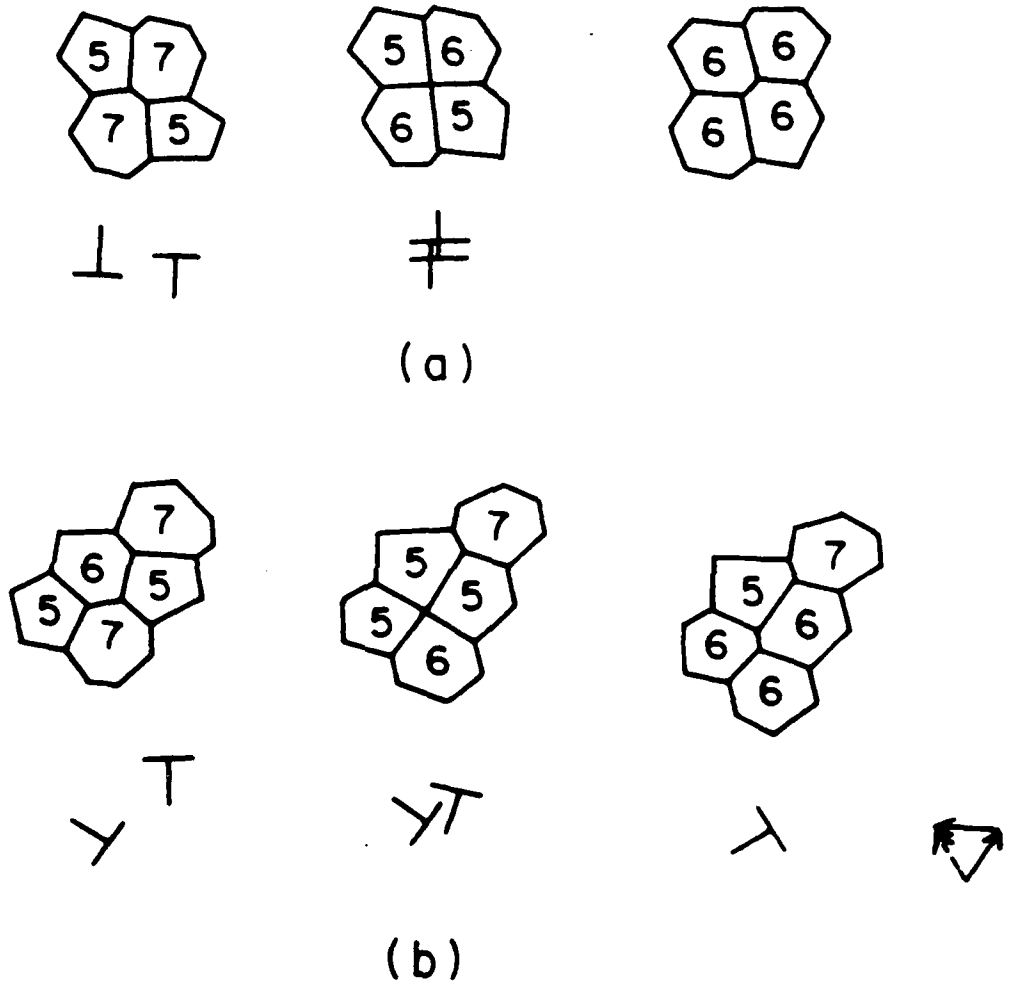


Fig. 7 - Two sequences of cancellation of dipoles: (a) dipole cancellation analogous to two opposite edge dislocation cores, (b) dipole reduction analogous to reaction of two 60° edge dislocation cores.

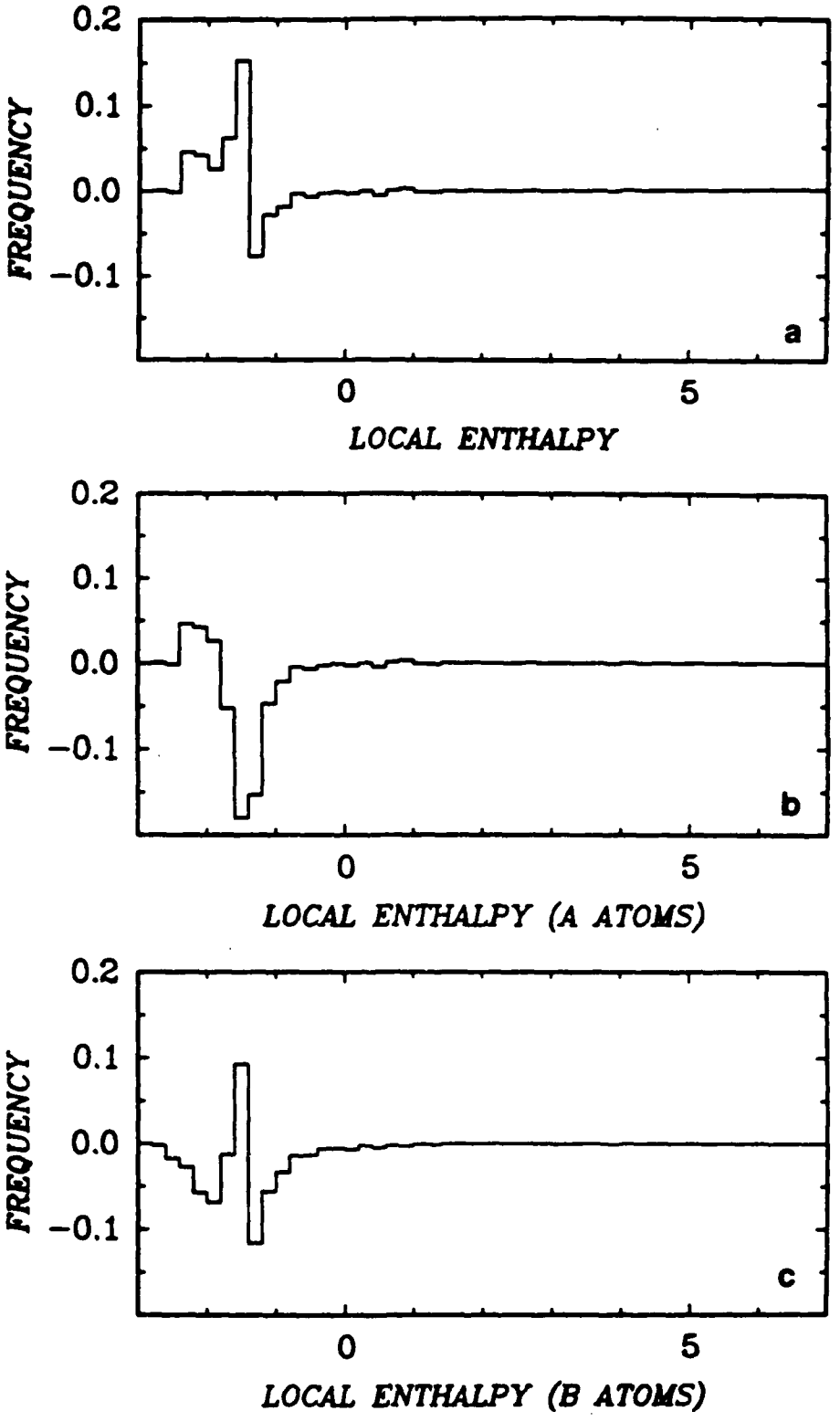


Fig. 8 - Total incremental effect of structural relaxation at $T^* = 0.1$ on atomic level enthalpy: (a) all atoms, (b) Cu atoms only, and (c) Zr atoms only.

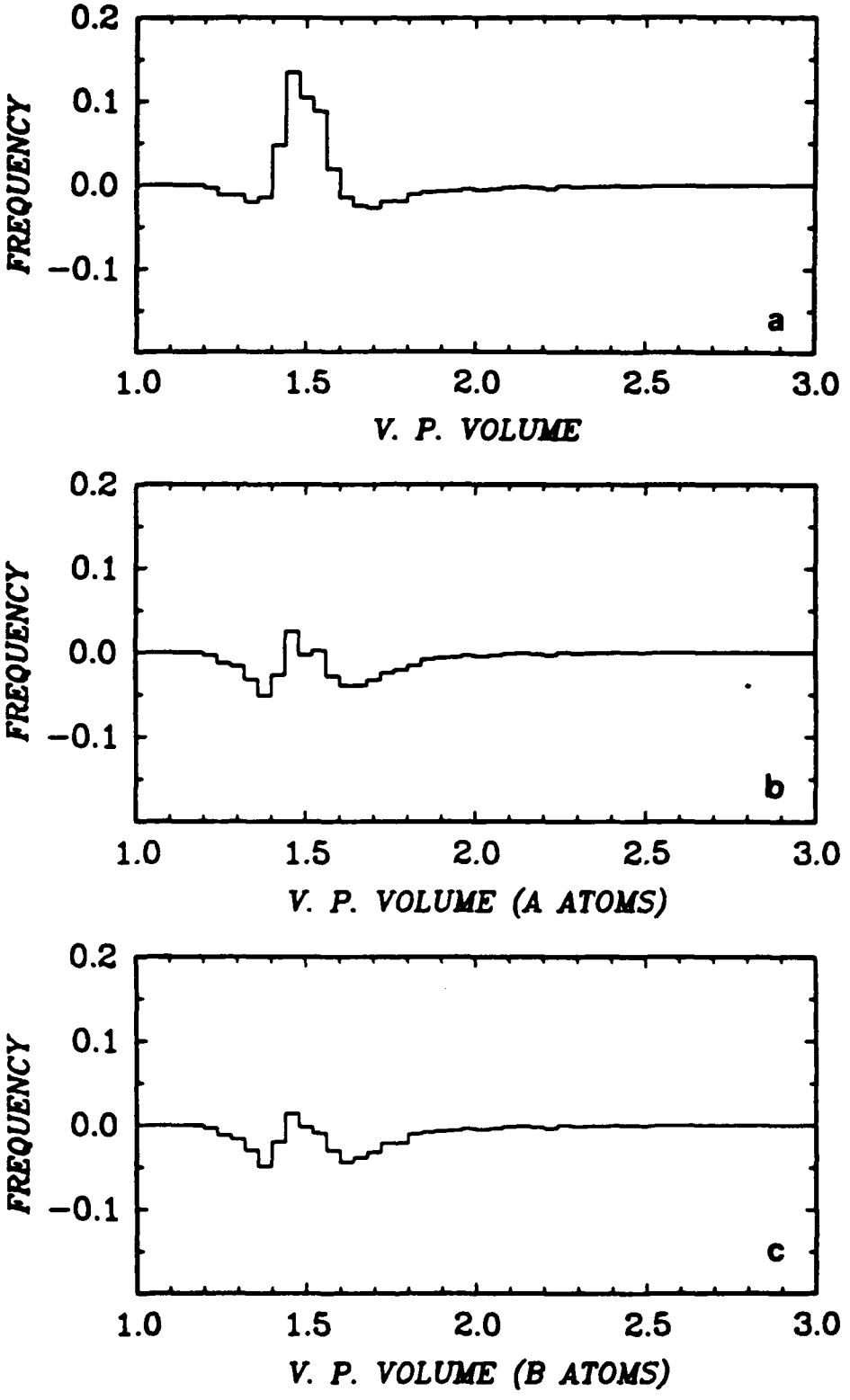


Fig. 9 - Total incremental effect of structural relaxation at $T^* = 0.1$ on volume per atom (Voronoi polygon volume): (a) all atoms, (b) Cu atoms only, and (c) Zr atoms only.

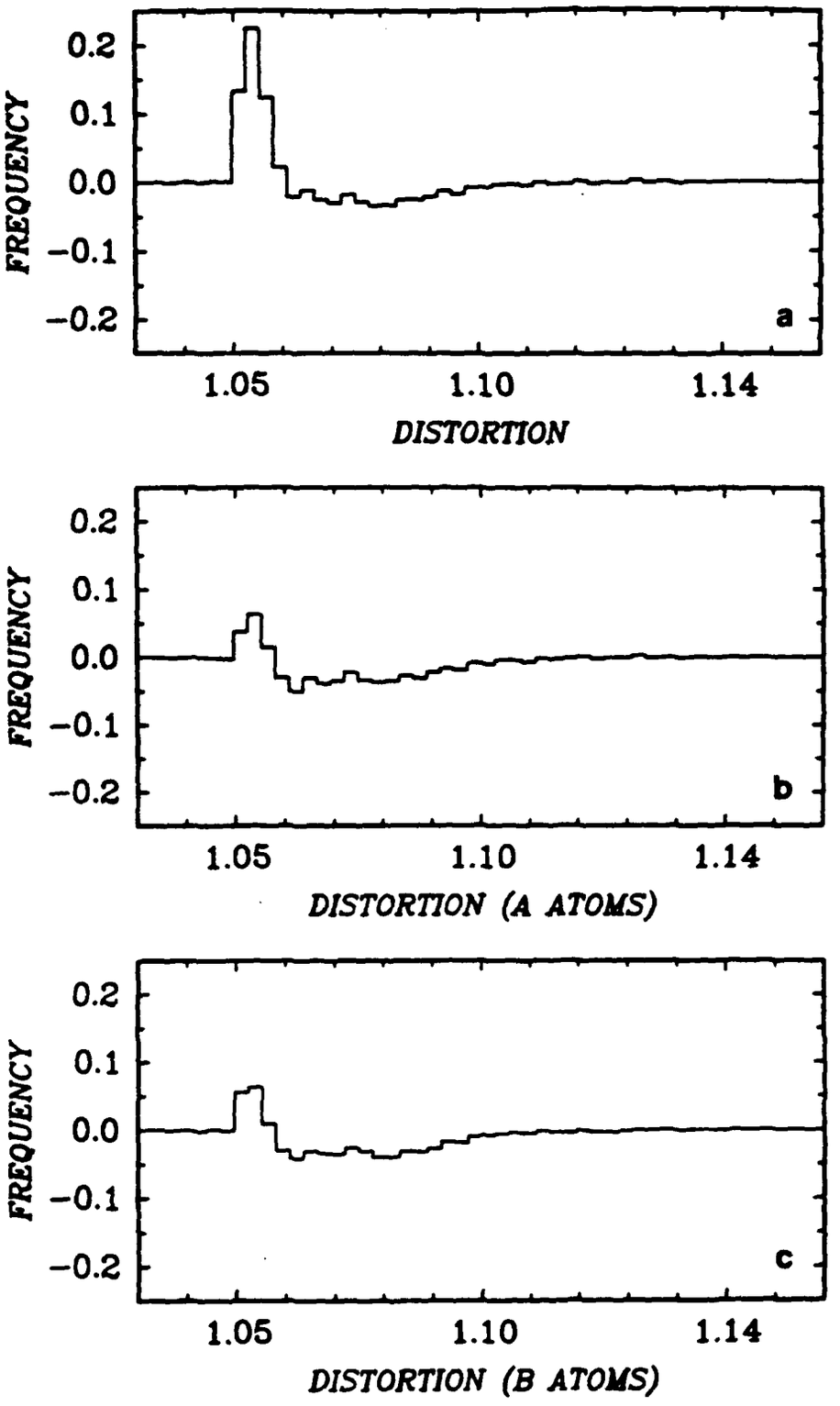


Fig. 10 - Total incremental effect of structural relaxation at $T^* = 0.1$ on atomic site distortion parameter: (a) all atoms, (b) Cu atoms only, and (c) Zr atoms only.

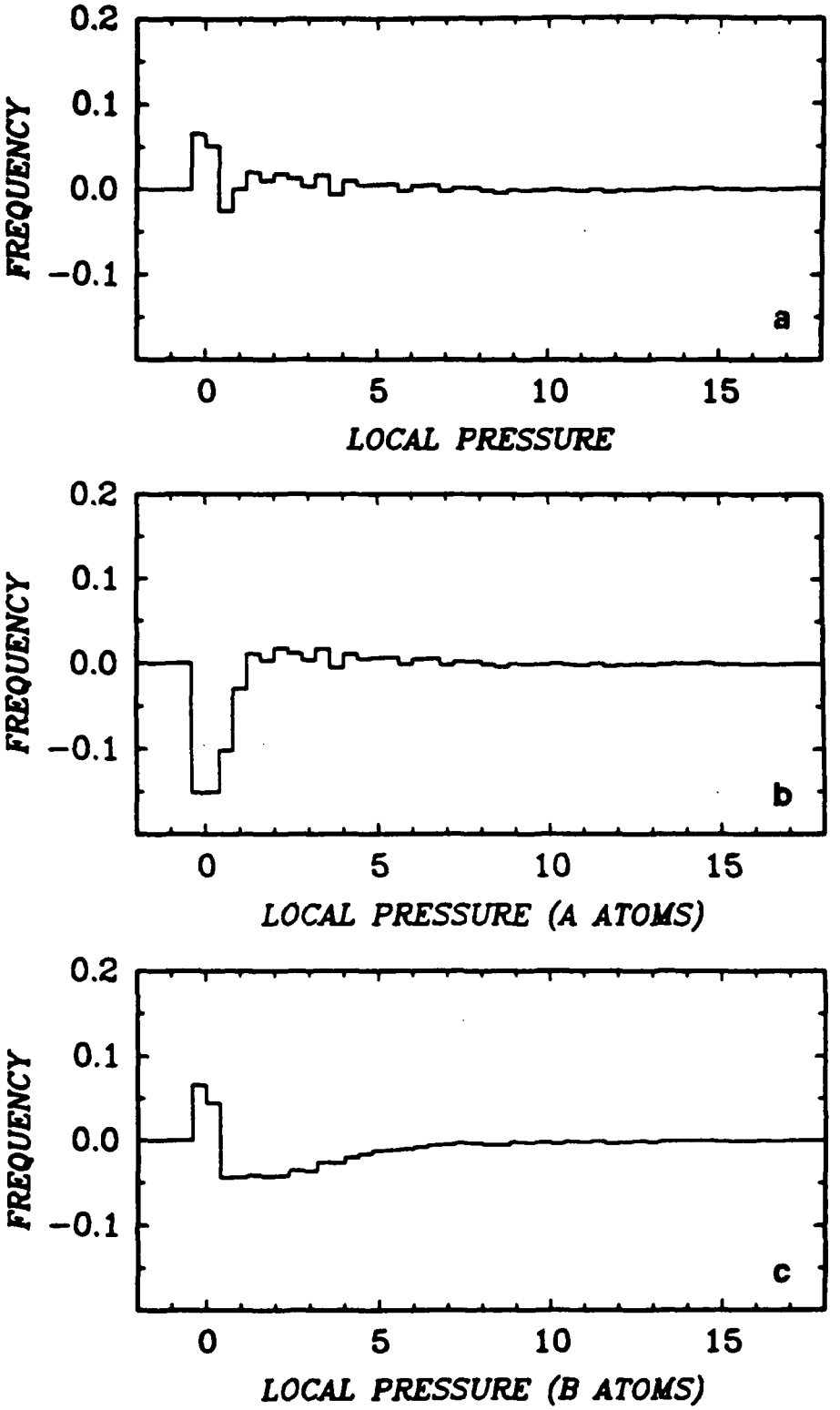


Fig. 11 - Total incremental effect of structural relaxation at $T^* = 0.1$ on atomic level pressure: (a) all atoms, (b) Cu atoms only, and (c) Zr atoms only.

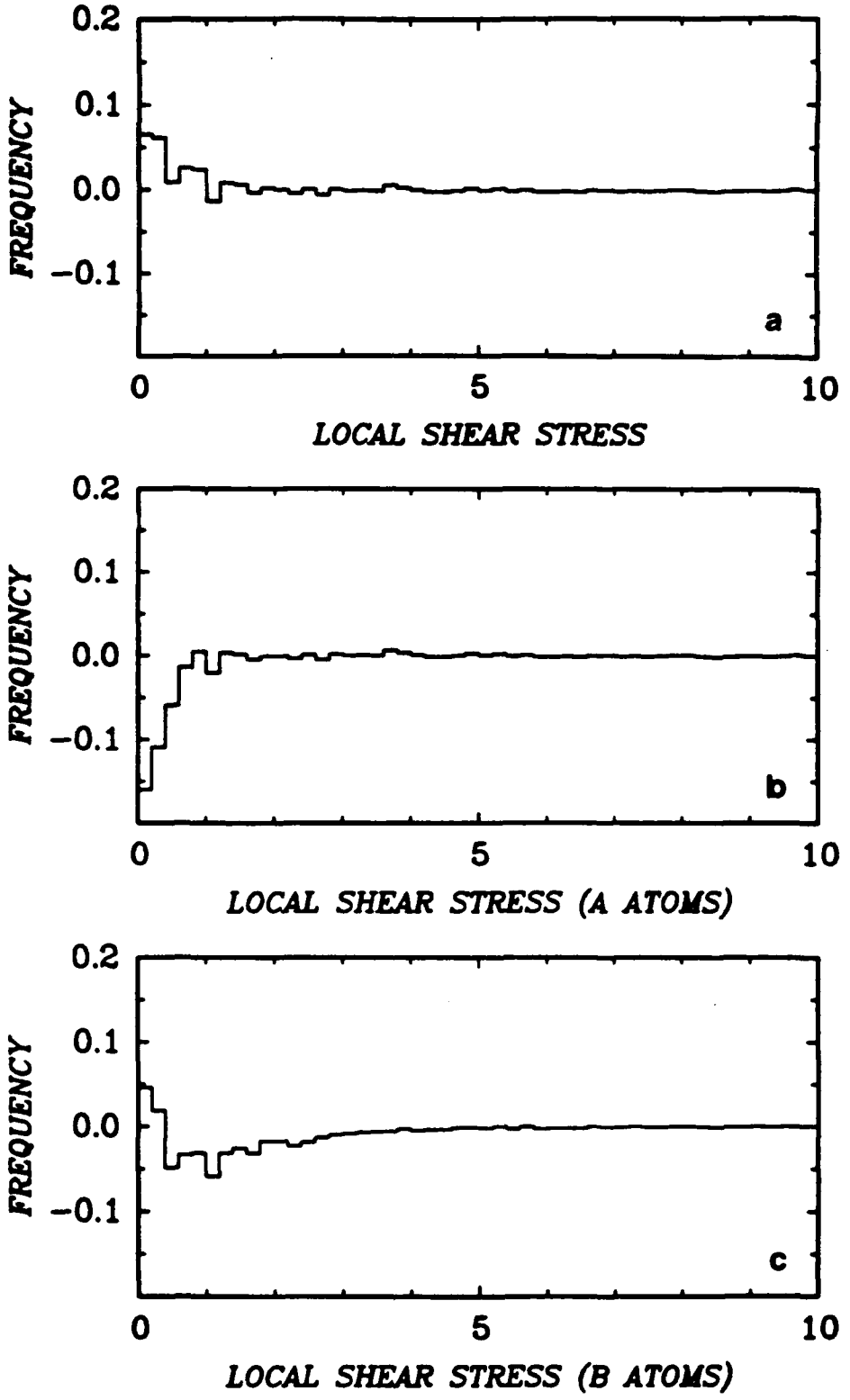


Fig. 12 - Total incremental effect of structural relaxation at $T^* = 0.1$ on atomic level maximum shear stress: (a) all atoms, (b) Cu atoms only, and (c) Zr atoms only.

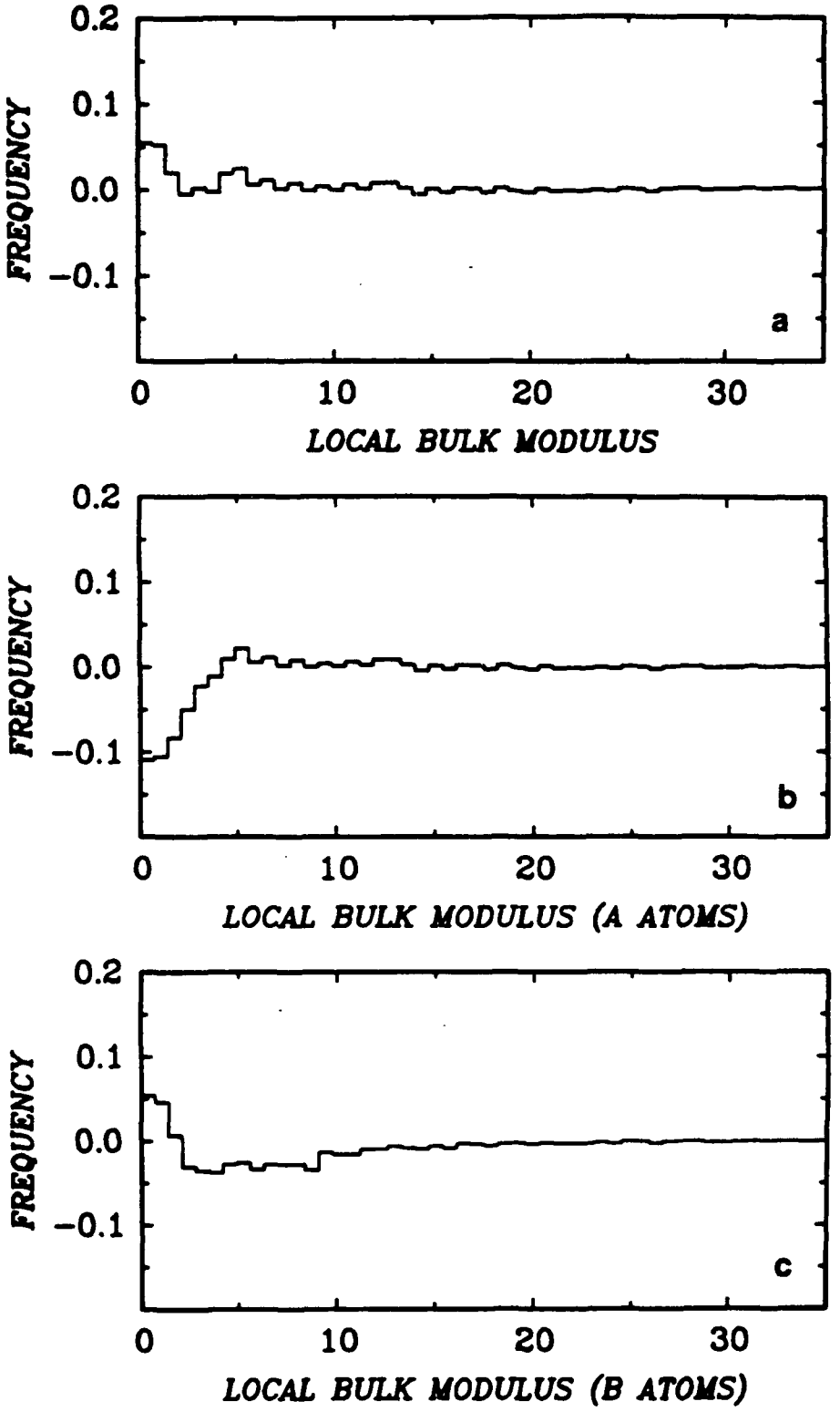


Fig. 13 - Total incremental effect of structural relaxation at $T^* = 0.1$ on atomic level bulk modulus: (a) all atoms, (b) Cu atoms only, and (c) Zr atoms only.

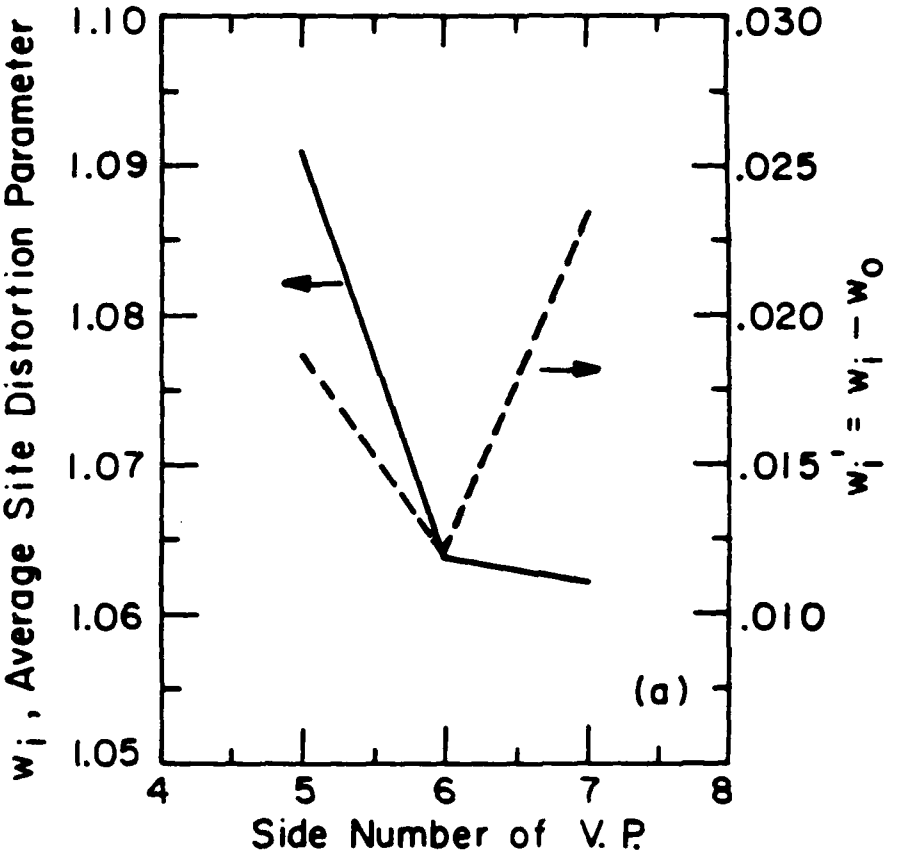


Fig. 14 - Comparison of intensive properties of polygons with six, five, and seven sides for partially relaxed mats at $\bar{T}^* = 0.1$: (a) corrected distortion parameter for average hexagon is less than those for average pentagon and heptagon, (b) atomic level enthalpy is lower for hexagons than for pentagons and heptagons.

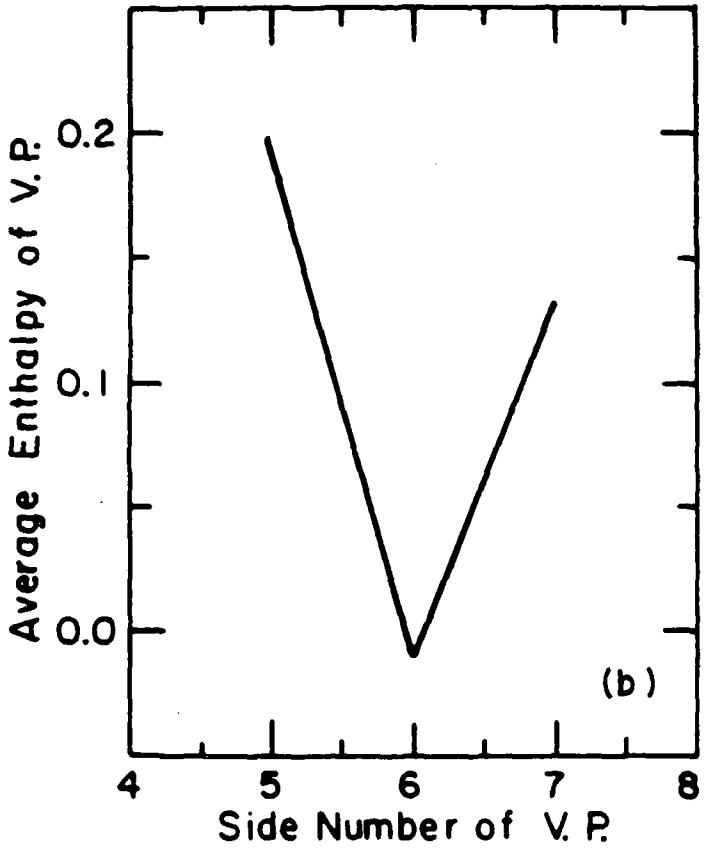


Fig. 14b